DOI: 10.1021/ic100383p

Inorganic Chemistry
Article

# Syntheses and Multi-NMR Study of *fac*- and *mer*-$OsO_3F_2(NCCH_3)$ and the X-ray Crystal Structure ($n$ = 2) and Raman Spectrum ($n$ = 0) of *fac*-$OsO_3F_2(NCCH_3)\cdot nCH_3CN$

**Michael J. Hughes, Michael Gerken,† Hélène P. A. Mercier, and Gary J. Schrobilgen***

*Department of Chemistry, McMaster University, Hamilton, Ontario, L8S 4M1, Canada. †Present address: Department of Chemistry and Biochemistry, The University of Lethbridge, Lethbridge AB T1K 3M4, Canada*

Received February 25, 2010

Dissolution of the infinite chain polymer, $(OsO_3F_2)_\infty$, in $CH_3CN$ solvent at −40 °C followed by solvent removal under vacuum at −40 °C yielded *fac*-$OsO_3F_2(NCCH_3)\cdot nCH_3CN$ ($n \geq 2$). Continued pumping at −40 °C with removal of uncoordinated $CH_3CN$ yielded *fac*-$OsO_3F_2(NCCH_3)$. Both *fac*-$OsO_3F_2(NCCH_3)\cdot nCH_3CN$ and *fac*-$OsO_3F_2(NCCH_3)$ are yellow-brown solids and were characterized by low-temperature (−150 °C) Raman spectroscopy. The crystal structure (−173 °C) of *fac*-$OsO_3F_2(NCCH_3)\cdot 2CH_3CN$ consists of two co-crystallized $CH_3CN$ molecules and a pseudo-octahedral $OsO_3F_2\cdot NCCH_3$ molecule in which three oxygen atoms are in a facial arrangement and $CH_3CN$ is coordinated trans to an oxygen atom in an end-on fashion. The Os---N bond length (2.205(3) Å) is among the shortest M---N adduct bonds observed for a $d^0$ transition metal oxide fluoride. The $^{19}F$ NMR spectrum of $(OsO_3F_2)_\infty$ in $CH_3CN$ solvent (−40 °C) is a singlet (−99.6 ppm) corresponding to *fac*-$OsO_3F_2(NCCH_3)$. The $^1H$, $^{15}N$, $^{13}C$, and $^{19}F$ NMR spectra of $^{15}N$-enriched $OsO_3F_2(NCCH_3)$ were recorded in $SO_2ClF$ solvent (−84 °C). Nitrogen-15 enrichment resulted in splitting of the $^{19}F$ resonance of *fac*-$OsO_3F_2(^{15}NCCH_3)$ into a doublet ($^2J(^{15}N-^{19}F)$, 21 Hz). In addition, a doublet of doublets ($^2J(^{19}F_{ax}-^{19}F_{eq})$, 134 Hz; $^2J(^{15}N-^{19}F_{eq})$, 18 Hz) and a doublet ($^2J(^{19}F_{ax}-^{19}F_{eq})$, 134 Hz) were observed in the $^{19}F$ NMR spectrum that have been assigned to *mer*-$OsO_3F_2(^{15}NCCH_3)$; however, coupling of $^{15}N$ to the axial fluorine-on-osmium environment could not be resolved. The nitrogen atom of $CH_3CN$ is coordinated trans to a fluorine ligand in the *mer*-isomer. Quantum-chemical calculations at the SVWN and B3LYP levels of theory were used to calculate the energy-minimized gas-phase geometries, vibrational frequencies of *fac*- and *mer*-$OsO_3F_2(NCCH_3)$ and of $CH_3CN$. The relative stabilities of the *mer*- and *fac*-isomers have been determined and are in accordance with the solution NMR assignments.

## Introduction

The Lewis acid behavior of $(OsO_3F_2)_\infty$ has been established by the syntheses of the $Ag^+$,[1] $Cs^+$,[1,2] $K^+$,[1,2] $Na^+$,[2] $N(CH_3)_4^+$,[3] $NO^+$,[3] $Rb^+$,[2] $XeF_5^+$,[4] and $Xe_2F_{11}^+$[4] salts of *fac*-$OsO_3F_3^-$ from their respective fluorides. The facial geometry of $OsO_3F_3^-$ was determined from the vibrational spectra of the $Cs^+$, $K^+$, $Rb^+$, and $Na^+$ salts[2] and was confirmed by the X-ray crystal structure and Raman spectra of $[N(CH_3)_4][OsO_3F_3]$[3] and $[M][OsO_3F_3]$ ($M = XeF_5^+$, $Xe_2F_{11}^+$).[4]

Acetonitrile forms Lewis base adducts with high-oxidation state $d^0$ transition metal fluorides $[CH_3CN\cdot MF_4(NCl)]$ ($M = Mo$,[5] W[6]), oxide fluorides $MoOF_4(NCCH_3)$,[7] $ReO_2F_3(NCCH_3)$,[8] $TcO_2F_3(NCCH_3)$,[9] and $WOF_4(NCCH_3)$,[10] as well as with the sulfide fluoride, $WSF_4(NCCH_3)$.[11] The crystal structures of $[CH_3CN\cdot MF_4(NCl]$ ($M = Mo$,[5] W[6]) and $ReO_3F(NCCH_3)_2\cdot CH_3CN$[8] have $CH_3CN$ coordinated to the $d^0$ metal through the nitrogen electron lone pair to give linear M---N−C−C arrangements. Both $CH_3CN$ ligands of $ReO_3F(NCCH_3)_2\cdot CH_3CN$[8] coordinate cis to one another and trans to

*To whom correspondence should be addressed. E-mail: schrobil@mcmaster.ca.

(1) Hepworth, M. A.; Robinson, P. L. J. *Inorg. Nucl. Chem.* **1957**, *4*, 24–29.
(2) Jones, P. J.; Levason, W.; Tajik, M. *J. Fluorine Chem.* **1984**, *25*, 195–201.
(3) Gerken, M.; Dixon, D. A.; Schrobilgen, G. J. *Inorg. Chem.* **2000**, *39*, 4244–4255.
(4) Hughes, M. J.; Mercier, H. P. A.; Schrobilgen, G. J. *Inorg. Chem.* **2010**, *49*, 3501−3515.
(5) Fenske, D.; Völp, K.; Dehnicke, K. *Z. Naturforsch., B: Chem. Sci.* **1987**, *42*, 1398–1402.
(6) Rhiel, M.; Wocadlo, S.; Massa, W.; Dehnicke, K. *Z. Anorg. Allg. Chem.* **1996**, *622*, 1195–1199.
(7) Buslaev, I. A.; Kokunov, Y. V.; Bochkaryova, V. A.; Shustorovich, E. M. *J. Inorg. Nucl. Chem.* **1972**, *34*, 2861–2865.
(8) Casteel, W. J.; Dixon, D. A.; LeBlond, N.; Lock, P. E.; Mercier, H. P. A.; Schrobilgen, G. J. *Inorg. Chem.* **1999**, *38*, 2340–2358.
(9) Casteel, W. J.; Dixon, D. A.; LeBlond, N.; Mercier, H. P. A.; Schrobilgen, G. J. *Inorg. Chem.* **1998**, *37*, 340–353.
(10) Buslaev, I. A.; Kokunov, Y. V.; Bochkareva, V. A. *J. Struct. Chem.* **1972**, *13*, 560–575; *Zh. Strukt. Khim.* **1972**, *13*, 611−616.
(11) Nieboer, J.; Hillary, W.; Yu, X.; Mercier, H. P. A.; Gerken, M. *Inorg. Chem.* **2009**, *48*, 11251–11258.


Published on Web 04/12/2010

two of the three facial oxygen atoms. The only examples of Os(VIII) coordinated to nitrogen are adducts of $OsO_4$, e.g., $OsO_4(NH_3)$,[12] $OsO_4(NC_5H_5)$,[13] $OsO_4(NC_7H_{13})$,[14] and $OsO_4L$ (L = $NC_9H_7$, $N_2C_8H_6$, and 1,2-$C_4H_4N_2$),[15] as well as nitrido-derivatives, e.g., [A][$OsO_3N$] (A = $(C_6H_5)_4As^+$,[16] $Cs^+$,[17] $K^+$,[18,19] and $H^+$[12]), $OsNCl_3(PPh_3)_2$,[20] and $OsO_2(OH)N$.[21] Prior to this work, there were no examples of nitrogen bases coordinated to Os(VIII) oxide fluorides known.

The current work describes the synthesis and characterization by multi-NMR and Raman spectroscopy, and single-crystal X-ray diffraction of *fac*-$OsO_3F_2(NCCH_3)$. The *mer*-$OsO_3F_2(NCCH_3)$ isomer in which the oxygen atoms are in a meridional arrangement and the $CH_3CN$ ligand is coordinated trans to fluorine has also been characterized in solution by multi-NMR spectroscopy along with *fac*-$OsO_3F_2(NCCH_3)$.

## Results and Discussion

**Syntheses of *fac*-$OsO_3F_2(NCCH_3)$, *fac*-$OsO_3F_2(NCCH_3)\cdot n CH_3CN$ ($n \geq 2$), and *mer*-$OsO_3F_2(NCCH_3)$.** Osmium trioxide difluoride, $(OsO_3F_2)_\infty$, dissolves in $CH_3CN$ at −40 °C according to eq 1 to give an orange-brown solution.

$$OsO_3F_2 + CH_3CN \xrightarrow[-40°C]{CH_3CN} fac\text{-}OsO_3F_2(NCCH_3) \quad (1)$$

Removal of excess $CH_3CN$ under dynamic vacuum at −40 °C initially yielded yellow-brown *fac*-$OsO_3F_2(NCCH_3)\cdot n CH_3CN$, which was confirmed by X-ray crystallography and Raman spectroscopy (Supporting Information, Table S1). Acetonitrile in the crystal lattice was removed by continued pumping for 3 h at −40 °C to yield yellow-brown *fac*-$OsO_3F_2(NCCH_3)$ (see Raman Spectroscopy) which did not dissociate after a further 3 h of pumping at −40 °C. The unsolvated complex is stable at room temperature for at least several days and is very soluble in $CH_3CN$ at −40 °C and slightly soluble in $SO_2ClF$ at −40 and −80 °C. The solution NMR spectra (see NMR Spectroscopy) revealed the presence of *fac*-$OsO_3F_2(NCCH_3)$ as the major product, but also the presence of *mer*-$OsO_3F_2(NCCH_3)$. Removal of excess $SO_2ClF$ under dynamic vacuum at −80 °C yielded only *fac*-$OsO_3F_2(NCCH_3)$ (Supporting Information, Table S1).

**X-ray Crystal Structure of *fac*-$OsO_3F_2(NCCH_3)\cdot 2CH_3CN$.** Details of the data collection parameters and other crystallographic information are provided in Table 1. Bond lengths and bond angles are listed in Table 2.

**Table 1.** Summary of Crystal Data and Refinement Results for *fac*-$OsO_3F_2(NCCH_3)\cdot 2CH_3CN$

| | |
|---|---|
| chem formula | $C_6F_2H_9N_3O_3Os$ |
| space group | *Pnma* (No. 62) |
| *a* (Å) | 7.7995(2) |
| *b* (Å) | 14.7327(4) |
| *c* (Å) | 9.5210(2) |
| *V* (Å$^3$) | 1095.2(1) |
| molecules/unit cell | 4 |
| mol wt (g mol$^{-1}$) | 1597.45 |
| calcd density (g cm$^{-3}$) | 2.425 |
| *T* (°C) | −173 |
| $\mu$ (mm$^{-1}$) | 11.68 |
| $R_1$[a] | 0.0178 |
| $wR_2$[b] | 0.0413 |

[a] $R_1$ is defined as $\sum||F_o| - |F_c||/\sum|F_o|$ for $I > 2\sigma(I)$. [b] $wR_2$ is defined as $\{\sum w(F_o^2 - F_c^2)^2/\sum w(F_o^2)^2\}^{1/2}$ for $I > 2\sigma(I)$.

The crystal structure (Figure 1a) is comprised of monomeric $OsO_3F_2$ coordinated to a $CH_3CN$ molecule through the nitrogen atom to give pseudo-octahedral coordination at osmium. In addition, there are two uncoordinated, symmetry-related $CH_3CN$ molecules in the asymmetric unit. The $OsO_3F_2(NCCH_3)$ adduct possesses a *fac*-trioxo arrangement about osmium in which the nitrogen atom of $CH_3CN$ is coordinated trans to an oxygen atom. Preference for the *fac*-trioxo arrangement has been well documented and is consistent with other $d^0$ transition metal trioxo species such as the related Os(VIII) and Re(VII) species, $(OsO_3F_2)_\infty$,[22] $(OsO_3F_2)\cdot 2XeOF_4$,[23] $OsO_3F_3^-$,[3,4] $[XeF_5][\mu\text{-}F(OsO_3F_2)_2]$,[4] $[OsO_3F][HF][SbF_6]$,[24] $ReO_3F$,[25] and $ReO_3F(CH_3CN)_2\cdot CH_3CN$,[8] and has been previously discussed.[3]

The crystal lattice consists of *fac*-$OsO_3F_2(NCCH_3)$ and $CH_3CN$ molecules stacked along the *b*- and *c*-axes which alternate along the *a*-axis (Supporting Information, Figure S1). In the *a*,*b*-plane, the adduct molecule reverses orientation between successive layers, with the free $CH_3CN$ molecules alternating their orientations in a similar manner. The resulting intermolecular contacts are long and are near the sums of the van der Waals radii of the contacting atoms.[26,27]

The C−N (1.140(5) Å) and C−C (1.437(5) Å) bond lengths of the adducted $CH_3CN$ molecule are comparable to those of the co-crystallized $CH_3CN$ solvent molecules (1.140(4) and 1.450(4) Å, respectively) and both bond lengths are similar to those of $ReO_3F(NCCH_3)_2$ (C−C 1.451(7), C−N 1.136(7) Å).[8] The C−N triple bond length is in good agreement with the previously

(12) Hair, M. L.; Robinson, P. L. *J. Chem. Soc.* **1960**, 2775–2776.
(13) Griffith, W. P.; Rossetti, R. *J. Chem. Soc., Dalton Trans.* **1972**, 1449–1453.
(14) Griffith, W. P.; Skapski, A. C.; Woode, K. A.; Wright, M. P. *Inorg. Chim. Acta* **1978**, *31*, L413–L414.
(15) Cleare, M. J.; Hydes, P. C.; Griffith, W. P.; Wright, M. P. *J. Chem. Soc., Dalton Trans.* **1977**, 941–944.
(16) Müller, V. A.; Bollmann, F.; Baran, E. J. *Z. Anorg. Allg. Chem.* **1969**, *370*, 238–247.
(17) Pastuszak, R.; L'Haridon, P.; Marchand, R.; Laurent, Y. *Acta Crystallogr., Sect B.* **1982**, *38*, 1427–1430.
(18) Clifford, A. F.; Kobayashi, C. S. *Inorg. Synth.* **1960**, *6*, 204–208.
(19) Schmidt, K. H.; Flemming, V.; Müller, A. *Spectrochim. Acta, Part A* **1975**, *31*, 1913–1919.
(20) Griffith, W. P.; Pawson, D. *J. Chem. Soc., Chem. Commun.* **1973**, 418–419.
(21) Griffith, W. P. *J. Chem. Soc.* **1965**, 3694–3697.
(22) Bougon, R.; Buu, B.; Seppelt, K. *Chem. Ber.* **1993**, *126*, 1331–1336.
(23) Hughes, M. J.; Mercier, H. P. A.; Schrobilgen, G. J. *Inorg. Chem.* **2009**, *48*, 4478–4490.
(24) Gerken, M.; Dixon, D. A.; Schrobilgen, G. J. *Inorg. Chem.* **2002**, *41*, 259–277.
(25) Supel, J.; Marx, R.; Seppelt, K. *Z. Anorg. Allg. Chem.* **2005**, *631*, 2979–2986.
(26) Bondi, A. *J. Phys. Chem.* **1964**, *68*, 441–451.
(27) The long contacts in *fac*-$OsO_3F_2(NCCH_3)$ are as follows: F(2)···O(2A) (2.988(3) Å), F(1)···H(5B) (2.469 Å) to F(2)···H(3C) (2.740 Å), O(1)···O(3D) (2.897(3) Å), O(3)···H(9D) (2.557 Å) to O(3)···H(1E) (2.861 Å), O(3)···C(2E) (3.094(4) Å), N(3)···H(1F) (2.601 Å), N(3)···C(1F) (3.206(5) Å) to N(3)···C(2G) (3.434(5) Å), and C(1)···C(5F) (3.471(5) Å). The corresponding sums of the van der Waals radii (taken from ref 26) are as follows: [F···F (2.94 Å), F···O (2.99 Å), F···N (3.02 Å), F···H (2.67 Å), F···C (3.17 Å), O···O (3.04 Å), O···N (3.07 Å), O···H (2.72 Å), O···C (3.22 Å), N···N (3.10 Å), N···H (2.75 Å), N···C (3.25 Å), H···H (2.40 Å), H···C (2.90 Å) and C···C (3.40 Å)].

**Table 2.** Experimental Geometrical Parameters for *fac*-$OsO_3F_2(NCCH_3)\cdot 2CH_3CN$ and Calculated Geometrical Parameters for *fac*-$OsO_3F_2(NCCH_3)$, *mer*-$OsO_3F_2(NCCH_3)$, and $CH_3CN$

| exptl[a] | | calcd | | | | | |
|---|---|---|---|---|---|---|---|
| *fac*-$OsO_3F_2(NCCH_3)\cdot 2CH_3CN$ | | *fac*-$OsO_3F_2(NCCH_3)$ ($C_1$) | | *mer*-$OsO_3F_2(NCCH_3)$ ($C_1$) | | $CH_3CN$ ($C_{3v}$) | |
| | | SVWN[b] | B3LYP[c] | SVWN[b] | B3LYP[c] | SVWN[b] | B3LYP[d] |
| | | | | Bond Lengths (Å) | | | |
| Os−O(1) | 1.704(2) | $Os-O_1$ | 1.727 | 1.701 | 1.760 | 1.736 | |
| | | $Os-O_2$ | 1.727 | 1.701 | 1.728 | 1.705 | |
| Os−O(2) | 1.696(2) | $Os-O_3$ | 1.712 | 1.687 | 1.760 | 1.736 | |
| Os−F(1) | 1.940(1) | $Os-F_1$ | 1.922 | 1.922 | 1.863 | 1.857 | |
| | | $Os-F_2$ | 1.922 | 1.922 | 1.968 | 1.972 | |
| Os---N(1) | 2.206(3) | Os---N | 2.260 | 2.386 | 2.114 | 2.175 | |
| N(1)−C(1) | 1.140(5) | $N-C_1$ | 1.169 | 1.142 | 1.167 | 1.140 | 1.181 | 1.149 |
| C(1)−C(2) | 1.437(5) | $C_1-C_2$ | 1.443 | 1.449 | 1.440 | 1.447 | 1.451 | 1.455 |
| C(2)−H | 0.980 | $C_2-H$ | 1.108 | 1.089 | 1.108 | 1.089 | 1.108 | 1.089 |
| N(2)−C(3) | 1.140(4) | | | | | | | |
| C(3)−C(4) | 1.456(4) | | | | | | | |
| C(4)−H | 0.94(4) | | | | | | | |
| | | | | Bond Angles (deg) | | | |
| O(1)−Os−O(1A) | 101.5(1) | $O_1-Os-O_2$ | 100.9 | 100.7 | 101.5 | 101.4 | | |
| O(1)−Os−O(2) | 102.60(8) | $O_1-Os-O_3$ | 103.4 | 103.5 | 101.5 | 100.4 | | |
| O(1)−Os−F(1) | 87.79(8) | $O_1-Os-F_1$ | 87.6 | 87.3 | 88.5 | 90.5 | | |
| O(1)−Os−F(1A) | 159.89(8) | $O_1-Os-F_2$ | 156.1 | 155.6 | 79.3 | 79.5 | | |
| O(1)−Os---N(1) | 84.08(7) | $O_1-Os---N_1$ | 82.9 | 82.0 | 91.0 | 88.9 | | |
| O(1A)−Os−O(2) | 102.60(8) | $O_2-Os-O_3$ | 103.4 | 103.5 | 156.9 | 158.7 | | |
| O(1A)−Os−F(1) | 159.89(8) | $O_2-Os-F_1$ | 156.1 | 155.6 | 88.5 | 90.5 | | |
| O(1A)−Os−F(1A) | 87.79(8) | $O_2-Os-F_2$ | 87.6 | 87.3 | 79.3 | 79.5 | | |
| O(1A)−Os---N(1) | 84.08(7) | $O_2-Os---N_1$ | 82.9 | 82.0 | 91.0 | 88.9 | | |
| O(2)−Os−F(1) | 92.52(8) | $O_3-Os-F_1$ | 96.2 | 96.8 | 100.1 | 100.0 | | |
| O(2)−Os−F(1A) | 92.52(8) | $O_3-Os-F_2$ | 96.2 | 96.8 | 155.8 | 158.4 | | |
| O(2)−Os---N(1) | 169.2(1) | $O_3-Os---N_1$ | 169.9 | 171.2 | 82.4 | 83.1 | | |
| F(1)−Os−F(1A) | 78.27(9) | $F_1-Os-F_2$ | 76.7 | 76.9 | 104.1 | 101.5 | | |
| F(1)−Os---N(1) | 79.16(7) | $F_1-Os---N_1$ | 75.9 | 76.3 | 177.5 | 176.9 | | |
| F(1A)−Os---N(1) | 79.16(7) | $F_2-Os---N_1$ | 75.9 | 76.3 | 73.4 | 75.4 | | |
| Os---N(1)−C(1) | 178.7(2) | $Os---N_1-C_1$ | 170.5 | 173.7 | 173.6 | 174.3 | | |
| N(1)−C(1)−C(2) | 178.6(3) | $N_1-C_1-C_2$ | 179.3 | 179.7 | 179.1 | 179.5 | | |
| C(1)−C(2)−H | 109.5 | $C_1-C_2-H$ | 110.0 | 110.3 | 110.0 | 109.3 | | |
| H−C(2)−H | 109.5 | $H-C_2-H$ | 108.5 | 109.0 | 108.5 | 109.4 | | |
| N(2)−C(3)−C(4) | 178.6(3) | | | | | | 180 | 180 |
| C(3)−C(4)−H(4A) | 111(3) | | | | | | 110.8 | 110.2 |
| C(3)−C(4)−H(4B) | 109(2) | | | | | | 108.1 | 108.8 |
| C(3)−C(4)−H(4C) | 109(2) | | | | | | | |
| H(4A)−C(4)−H(4B) | 109(3) | | | | | | | |
| H(4A)−C(4)−H(4C) | 115(3) | | | | | | | |
| H(4B)−C(4)−H(4C) | 104(3) | | | | | | | |

[a] For the atom labeling scheme, see Figure 1a. [b] The SDDall basis set, augmented for F and O with two d-type polarization functions by Huzinaga, was used.[56] [c] The Stuttgart basis set for Os augmented with one f-type polarization functional was used;[57] The aug-cc-pVTZ basis sets were used for all other atoms. [d] The aug-cc-pVTZ basis set was used.

calculated additive covalent radii for C (0.60 Å) and N (0.54 Å).[28]

The Os---N bond length (2.206(3) Å) is shorter than the metal-nitrogen bond lengths of the $d^0$ rhenium and tungsten adducts, $ReO_3F(NCCH_3)_2\cdot CH_3CN$ (2.294(4) Å),[8] $WF_6(NC_5H_4F)$ (2.294(9) Å),[29] $WOF_4(NC_5H_4F)$ (2.39(1) Å),[29] and $WOF_4(NC_5H_5)$ (2.246(8) Å).[30] The nitrogen atom is trans to an oxygen atom which is consistent with the latter adducts and fluorine-bridged oxide fluoride compounds where the weakly bonded bridging fluorine atom is trans to an oxygen atom; e.g., $(OsO_3F_2)_\infty$,[22] $(OsO_3F_2)_2\cdot 2XeOF_4$,[23] $\mu$-$F(OsO_3F_2)_2^-$,[4] $F(cis\text{-}OsO_2F_3)_2^+$,[31] polymeric $MO_2F_3\cdot SbF_5$ (M = Re, Tc),[32] $F(TcOF_4)_2^+$,[33] $F(ReOF_4)_2^+$,[34] $F(cis\text{-}ReO_2F_3)_2^+$,[8] $Re_3O_6F_{10}^-$,[9] $(WOF_4)_4$,[35] and $(MoOF_4)_\infty$.[36] The *trans*-influence of oxygen results in bonding of the nitrogen and fluorine atoms trans to oxygen atoms because the $CH_3CN$ and fluorine $\sigma$-donor ligands do not compete as effectively as the $\pi$-donor oxygen ligands for the osmium $d_{t_{2g}}$ orbitals.[9]

(28) Pyykkö, P.; Riedel, S.; Patzschke, M. *Chem.—Eur. J.* **2005**, *11*, 3511–3520.
(29) Arnaudet, L.; Bougon, R.; Buu, B.; Lance, M.; Nierlich, M.; Vigner, J. *Inorg. Chem.* **1993**, *32*, 1142–1146.
(30) Arnaudet, L.; Bougon, R.; Ban, B.; Charpin, P.; Isabey, J.; Lance, M.; Nierlich, M.; Vigner, J. *Inorg. Chem.* **1989**, *28*, 257–262.
(31) Casteel, W. J.; Dixon, D. A.; Mercier, H. P. A.; Schrobilgen, G. J. *Inorg. Chem.* **1996**, *35*, 4310–4322.
(32) LeBlond, N.; Dixon, D. A.; Schrobilgen, G. J. *Inorg. Chem.* **2000**, *39*, 2473–2487.
(33) LeBlond, N.; Mercier, H. P. A.; Dixon, D. A.; Schrobilgen, G. J. *Inorg. Chem.* **2000**, *39*, 4494–4509.
(34) Schrobilgen, G. J.; Holloway, J. H.; Russell, D. R. *J. Chem. Soc., Dalton Trans.* **1984**, 1411–1415.
(35) Edwards, A. J.; Jones, G. R. *J. Chem. Soc. A.* **1968**, 2074–2078.
(36) Edwards, A. J.; Steventon, B. R. *J. Chem. Soc. A.* **1968**, 2503–2510.

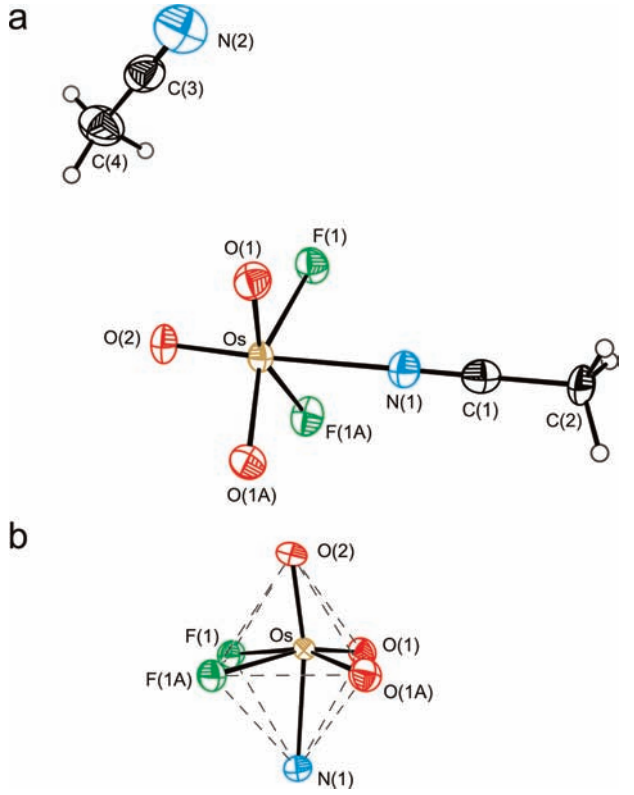


**Figure 1.** (a) Structural unit in the X-ray crystal structure of *fac*-$OsO_3F_2(NCCH_3)\cdot 2CH_3CN$ with thermal ellipsoids drawn at the 70% probability level. (b) The octahedron formed by the light atoms of the $OsO_3F_2N$-unit.

All Os−O bonds are *cis* to one another, and the bond lengths are equal to within $\pm 3\sigma$ (1.704(2) and 1.696(2) Å) and are in the same range as those of other neutral *fac*-trioxo osmium(VIII) compounds such as $(OsO_3F_2)_\infty$ (1.688(1), 1.678(1), and 1.727(1) Å),[22] and $(OsO_3F_2)_2\cdot 2XeOF_4$ (1.703(6), 1.685(6), and 1.685(6) Å).[23] Although the Os−N bond is longer than the Os−F bonds (vide infra), the Os−O(2) bond does not show significant shortening, indicating that, like fluorine, $CH_3CN$ does not compete as effectively with oxygen as a donor to osmium(VIII). The Os−F(1,1A) bonds (1.940(1) Å) are longer than the terminal Os−F bond in $(OsO_3F_2)_\infty$ (1.879(1) Å),[22] but are similar to those of the $OsO_3F_3^-$ anion (1.97(1)−1.91(1) Å),[3] suggesting that the adducted $CH_3CN$ molecule donates sufficient electron density to the osmium atom to significantly weaken the Os−F bonds (see Computational Results).

The ligand atoms of *fac*-$OsO_3F_2(NCCH_3)$ form a distorted octahedral coordination sphere around osmium. Although there is significant variation in the bond lengths around the osmium atom, the octahedron formed by the light atoms is relatively undistorted (Figure 1b), as shown by the range of nearest neighbor-ligand atom contacts.[37] The F(1), F(1A), O(1), and O(1A) [F(1), N(1), O(1A), and O(2)] {F(1A), N(1), O(1), and O(2)} atoms are coplanar

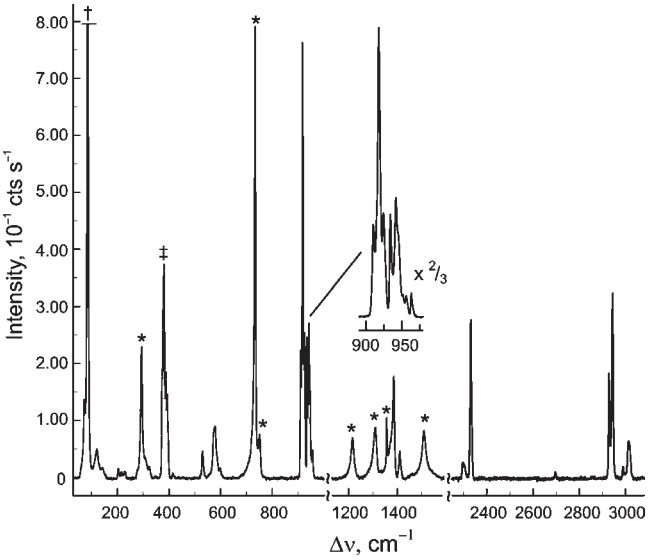


**Figure 2.** Raman spectrum of *fac*-$OsO_3F_2(NCCH_3)$ recorded at −150 °C using 1064-nm excitation; the symbols denote FEP sample tube lines (*), a band that overlaps with an FEP sample tube line (‡), and an instrumental artifact (†).

to within ±0.001 [0.03] {0.03} Å, and the osmium atom lies 0.255 [0.256] {0.159} Å out of this plane, toward O(2) [O(1)] {O(1A)}. All three planes are orthogonal to one another to within ±0.3°. The Os−O(2) and Os---N(1) bonds bend away from the Os−O(1,1A) bonds toward the Os−F(1,1A) bonds at an angle of 169.2(1)°. The displacement of the osmium atom toward the *fac*-$OsO_3$ group is similar to the metal atom displacements observed in $(OsO_3F_2)_\infty$,[22] $(OsO_3F_2)_2\cdot 2XeOF_4$,[23] $ReCl_3O_3^{2-}$,[38] $OsO_3F_3^-$,[3,4] and $\mu$-$F(OsO_3F_2)_2^{4-}$ and to those in the *cis*-dioxo-metal oxide fluoride species *cis*-$OsO_2F_4$,[39] F(*cis*-$OsO_2F_3)_2^+$,[31] $OsO_2F_3^+$,[40] *cis*-$ReO_2F_4^-$,[8] and *cis*-$TcO_2F_4^-$,[9] where the central metal atom is symmetrically displaced along the line bisecting the O−M−O angle toward the oxygen ligands of the *cis*-$MO_2$ group.

**Raman Spectroscopy.** The low-temperature Raman spectrum of *fac*-$OsO_3F_2(NCCH_3)$ (Figure 2) is very similar to that of *fac*-$OsO_3F_2(NCCH_3)\cdot n CH_3CN$, where $n \geq 2$ (Supporting Information, Figure S2), with the exception of the vibrational bands of uncoordinated $CH_3CN$. With few exceptions, the bands in both spectra are split into two components. The Raman spectrum of *fac*-$OsO_3F_2(NCCH_3)$ isolated from $SO_2ClF$ showed a small amount of free $CH_3CN$ as an impurity (Supporting Information, Table S1). The assigned Raman spectrum is that of the unsolvated product, *fac*-$OsO_3F_2(NCCH_3)$, whereas the crystal structure is that of the solvated product, *fac*-$OsO_3F_2(NCCH_3)\cdot 2CH_3CN$. Consequently, a factor-group analysis could not be carried out to unambiguously confirm that the additional splittings in the Raman spectra of *fac*-$OsO_3F_2(NCCH_3)$ and *fac*-$OsO_3F_2(NCCH_3)\cdot n CH_3CN$ arise from vibrational coupling within the unit cell. The factor-group analysis for *fac*-$OsO_3F_2(NCCH_3)\cdot 2CH_3CN$ (Supporting Information,

(37) The interatomic distances for the light atoms that comprise the coordination spheres of the Os atoms in *fac*-$OsO_3F_2(NCCH_3)$ are as follows: O(1)···O(2,3) 2.638(3), 2.655(3) Å; O(1)···F(1) 2.538(3) Å; O(1)···N(1) 2.647(4) Å; O(2)···O(3) 2.658(3); O(2)···F(2) 2.534(3) Å; O(2)···N(1) 2.646(4) Å; O(3)···F(1,2) 2.633(3), 2.636(3); and N(1)···F(1,2) 2.645(3), 2.647(3) Å.

(38) Lis, T. *Acta Crystallogr., Sect. C* **1983**, *39*, 961–962.
(39) Christe, K. O.; Dixon, D. A.; Mack, H. G.; Oberhammer, H.; Pagelot, A.; Sanders, J. C. P.; Schrobilgen, G. J. *J. Am. Chem. Soc.* **1993**, *115*, 11279–11284.
(40) Hughes, M. J.; Mercier, H. P. A.; Schrobilgen, G. J. *Inorg. Chem.* **2010**, *49*, 271–284.

**Table 3.** Calculated and Experimental Raman Frequencies, Intensities, and Assignments for *fac*-$OsO_3F_2(NCCH_3)$

| exptl[a] | | calcd | | | | assgnts ($C_1$)[f] |
|---|---|---|---|---|---|---|
| *fac*-$OsO_3F_2(NCCH_3)$ | $CH_3CN$ | *fac*-$OsO_3F_2(NCCH_3)$ | | $CH_3CN$ | | |
| | | SVWN[b,c] | B3LYP[c,d] | SVWN[b,c] | B3LYP[c,e] | |
| 3014(8), 2990(2) | 2999(54) | 3072(81)[3]<br>3071(74)[3] | 3125(67)[<1]<br>3125(64)[1] | 3065(64)[<1] | 3115(58)[1] | $\nu_{as}(CH_3)$ |
| 2944(43), 2929(24) | 2938(97) | 2976(230)[4] | 3052(239)[<1] | 2972(144)[1] | 3048(195)[3] | $\nu_s(CH_3)$ |
| 2697(1)[g] | | | | | | |
| 2332(36) | 2248(100) | 2322(245)[67] | 2422(184)[78] | 2247(50)[8] | 2363(81)[11] | $\nu$(CN) |
| 2296(3)[h] | | | | | | |
| 1410(6) | 1457(11)<br>1454(7) | 1425(20)[24] | 1467(6)[12] | 1439(21)[20] | 1475(5)[10] | $\delta_{as}(CH_3)$ |
| 1385(24) | 1425(3)<br>1420(4) | 1425(19)[24] | 1467(6)[12] | | | |
| 1356(14) | 1376(15)<br>1371(3) | 1394(34)[27] | 1411(12)[2] | 1397(18)[22] | 1413(6)[2] | $\delta_s(CH_3)$ |
| 1041(1), 1029(1) | 1042(1) | 1043(<1)[10]<br>1040(<0.1)[10] | 1063(<1)[4]<br>1061(<1)[4] | 1048(<1)[6] | 1063(<1)[2] | $\rho_r(CH_3)$ |
| 956(6), 952(sh) | 922(20) | 988(5)[16] | 1020(60)[95] | 948(5)[1] | 928(5)[1] | $\nu$(CC)[i] |
| 945(sh), 942(36) | | 951(37)[64] | 989(23)[125] | | | $\nu(OsO_1) + \nu(OsO_2)$ |
| 934(33), 924(34) | | 949(14)[117] | 975(14)[150] | | | $\nu(OsO_1) - \nu(OsO_2)$ |
| 918(100), 910(30) | | 983(47)[117] | 948(8)[9] | | | $\nu(OsO_3)$[j] |
| 598(2) | | 624(10)[98] | 609(8)[115] | | | $\nu(OsF_1) + \nu(OsF_2)$ |
| 529(7) | | 564(7)[52] | 547(4)[51] | | | $\nu(OsF_1) - \nu(OsF_2)$ |
| | 400(3) | 410(2)[<1] | 421(<1)[1] | | | $\delta(NCC)_{oop}$ |
| 415(1) | 395(12)<br>392(9)<br>386(5) | 408(2)[<1] | 422(1)[3] | 375(4)[<1] | 382(1)[1] | $\delta(NCC)_{ip}$ |
| 396(sh), 392(19) | | 387(4)[2] | 417(3)[2] | | | $\delta(O_1OsO_2) + \delta(F_1OsF_2)$ |
| 388(50)[k] | | 369(5)[13] | 392(1)[12] | | | $\delta(OsO_1O_2O_3)$ |
| 378(40), 374(sh) | | 361(6)[5] | 386(6)[6] | | | $\rho_t(O_1OsO_2) + \delta(O_2OsO_3)$ |
| 326(2) | | 319(<1)[10] | 338(<1)[10] | | | $\delta(O_1OsO_2) - \delta(F_1OsF_2) + \delta(NCC)_{ip\ small}$ |
| 309(4) | | 281(2)[13] | 289(2)[17] | | | $\delta(OsF_1F_2O_3)$ |
| 277(sh) | | 278(2)[17] | 291(2)[20] | | | $\rho_t(O_1OsO_2) - \rho_t(F_1OsF_2) + \delta(NCC)_{oop}$ |
| 232(1), 228(1) | | 217(<1)[<1] | 211(<1)[<1] | | | $\delta$(Os---NC)$_{ip}$ |
| 216(1) | | 214(<1)[<1] | 209(<1)[1] | | | $\delta$(Os---NC)$_{oop}$ |
| 204(2) | | 203(1)[16] | 149(<1)[17] | | | $\nu$(Os---N) |
| 143(2) | | 174(<1)[<0.1] | 174(<1)[<0.1] | | | $\rho_t(F_1OsF_2) - \rho_t(O_2OsO_1)$ |
| 121(7) | | 49(2)[5] | 50(1)[4] | | | $\rho_w(NCC)_{ip}$ |
| | | 49(2)[4] | 50(2)[4] | | | $\rho_w(NCC)_{oop}$ |
| n.o. | | 14(<0.1)[<0.1] | 5(<0.1)[<0.1] | | | $\rho_t(CH_3)$ |
| 230(1) | 116(18) | | | | | |
| 119(sh) | 108(13) | | | | | lattice modes |
| 114(11) | 102(15) | | | | | |
| 106(8) | 96(32) | | | | | |

[a] The Raman spectrum was recorded on a microcrystalline solid in a FEP sample tube at −150 °C using 1064-nm excitation. Raman intensities are given in parentheses and are relative intensities with the most intense band given as 100. The abbreviation (sh) denotes a shoulder. [b] SVWN/SDDall. [c] Values in parentheses denote calculated Raman intensities ($Å^4\ u^{-1}$) and values in square brackets denote calculated infrared intensities (km $mol^{-1}$). [d] B3LYP/Stutt-f (Os) aug-cc-pVTZ (H, C, N, F). [e] B3LYP/aug-cc-pVTZ (H,C,N). [f] Assignments are based on the B3LYP calculated geometry. The atom labeling scheme refers to Figure 4a for *fac*-$OsO_3F_2(NCCH_3)$, and the plane of symmetry is defined by the $O_2$, $O_3$, Os, $F_1$, and N atoms. The abbreviations denote stretch ($\nu$), bend ($\delta$), torsion ($\rho_t$), wag ($\rho_w$), rock ($\rho_r$), out-of-plane (oop), and in-plane (ip). [g] Overtone band corresponding to $2 \times 1356\ cm^{-1}$. [h] Combination band corresponding to $1356 + 956\ cm^{-1}$. [i] At the SVWN level, the mode description is $\nu(C_1C_2) - \nu(OsO_3)_{small}$. [j] At the SVWN level, the mode description is $\nu(OsO_3) + \nu(C_1C_2)_{small}$. [k] The band overlaps with a FEP sample tube band.

Table S2), however, predicts that the vibrational bands are split into two components, suggesting that the unit cells of *fac*-$OsO_3F_2(NCCH_3)$, *fac*-$OsO_3F_2(NCCH_3)\cdot nCH_3CN$, and *fac*-$OsO_3F_2(NCCH_3)\cdot 2CH_3CN$ are closely related, or identical for the solvated adducts, i.e., $n = 2$.

The observed and calculated frequencies of *fac*-$OsO_3F_2(NCCH_3)$ at both the SVWN and B3LYP levels of theory and their assignments are listed in Table 3. The spectral assignments were made by comparison with the calculated frequencies and Raman intensities (Table 3) of the energy-minimized geometries of *fac*-$OsO_3F_2(NCCH_3)$ and $CH_3CN$ (see Computational Results). The calculated vibrational frequencies obtained at the SVWN and B3LYP levels are in good agreement. The mode descriptions are based on the atomic displacements obtained for the optimized B3LYP geometry.

The bands at 924, 934 and at 942, 945 $cm^{-1}$ are assigned to the out-of-phase $\nu(OsO_1) - \nu(OsO_2)$ and the in-phase $\nu(OsO_1) + \nu(OsO_2)$ stretching modes. The modes are shifted to lower frequency when compared with the corresponding modes in $(OsO_3F_2)_\infty$ (945, 949, 952, 957 $cm^{-1}$),[23] in accordance with donation of electron density from the nitrogen atom to the osmium atom which weakens the Os−O bonds. The Os−O stretching modes occur to higher frequency than those of $OsO_3F_3^-$ (908, 912, 920 $cm^{-1}$),[3] consistent with the lower base strength of $CH_3CN$ relative to that of the fluoride ion. On the basis of the vibrational displacements obtained at the B3LYP level, the relatively strong bands at 910 and 918 $cm^{-1}$ are assigned to the $\nu(OsO_3)$ stretching mode; however, at the SVWN level, the $\nu(OsO_3)$ stretch weakly couples in an in-phase manner with $\nu(C_1C_2)$ of the $CH_3CN$ ligand bonded trans to $O_3$. The in-phase $\nu(OsF_1) + \nu(OsF_2)$ (598 $cm^{-1}$) stretching mode occurs to higher frequency than its out-of-phase counterpart, $\nu(OsF_1) - \nu(OsF_2)$ (529 $cm^{-1}$), in agreement with the calculated values (609 and 547 [B3LYP] $cm^{-1}$, respectively). The in-phase stretch is very similar to the in-phase stretch of $(OsO_3F_2)_\infty$

**Table 4.** NMR Chemical Shifts and Spin−Spin Coupling Constants for *fac*-$OsO_3F_2(^{14/15}NCCH_3)$ and *mer*-$OsO_3F_2(^{14/15}NCCH_3)$

| | | | chemical shifts, ppm | | | | coupling constants, Hz | | | |
|---|---|---|---|---|---|---|---|---|---|---|
| species | solvent | $T$ (°C) | $\delta(^{19}F)^a$ | $\delta(^{15}N)$ | $\delta(^{13}C)^b$ | $\delta(^1H)$ | $^2J(^{19}F_1-^{19}F_2)^a$ | $^1J(^{15}N-^{19}F_1)^a$ | $^1J(^{13}C-^1H)$ | $^1J(^{19}F-^{187}Os)^c$ |
| *fac*-$OsO_3F_2(^{14}NCCH_3)$ | $CH_3CN$ | −40 | −99.6[d] | | | 2.55[e] | | | 126.1 | |
| *fac*-$OsO_3F_2(^{14}NCCH_3)$ | $SO_2ClF^f$ | −40 | −93.6 | | | 2.66 | | | 137.9 | |
| *fac*-$OsO_3F_2(^{14}NCCH_3)$ | $SO_2ClF^f$ | −80 | −96.1 | | | 1.76 | | | 139.5 | 41.2 |
| *fac*-$OsO_3F_2(^{15}NCCH_3)^g$ | $SO_2ClF^f$ | −84 | −96.8 | −197.3 | 2.24 ($CH_3$) | 2.02 | | 21.4 | 139.8 | |
| *mer*-$OsO_3F_2(^{14}NCCH_3)$ | $SO_2ClF^f$ | −40 | −44.4 $F_2$<br>−13.1 $F_1$ | | | 3.12 | 134.3 | | 142.8 | |
| *mer*-$OsO_3F_2(^{14}NCCH_3)$ | $SO_2ClF^f$ | −80 | −46.1 $F_2$<br>−15.4 $F_1$ | | | 2.71 | 135.0 | | 145.3 | |
| *mer*-$OsO_3F_2(^{15}NCCH_3)^g$ | $SO_2ClF^f$ | −84 | −48.0 $F_2$<br>−17.9 $F_1$ | −258.6 | 3.15 ($CH_3$) | 3.04 | 134.3 | 18.3 | 140.4 | |

[a] The equatorial and axial fluorine atoms are denoted by $F_1$ and $F_2$, respectively. [b] The $^{13}C$ resonances of *fac*-$OsO_3F_2(^{14}NCCH_3)$ and *mer*-$OsO_3F_2(^{14}NCCH_3)$ could not be observed. [c] The $^1J(^{19}F-^{187}Os)$ coupling constant could only be observed for *fac*-$OsO_3F_2(^{14}NCCH_3)$ in $SO_2ClF$ solvent (−80 °C). [d] Weak doublet (46.9 ppm) and quintet (95.2 ppm) ($^2J(^{19}F-^{19}F)$ = 92 Hz) resonances assigned to $OsO_2F_5^-$ were observed in the $^{19}F$ spectrum. [e] Acetonitrile solvent was observed in the $^1H$ spectrum at 2.01 ppm, $^1J(^1H-^{13}C)$ = 137 Hz. [f] Resonances assigned to $SO_2ClF$ solvent, $SO_2F_2$ solvent impurity (parentheses), and weak unassigned resonances (braces) were observed in the $^{19}F$ spectra [−40 °C: 98.9 (32.7) {−70.5, −72.0, −76.6}; −80 °C: 98.5 (32.7) {−70.7, −72.2, −76.7}; −84 °C: 98.7 (32.7) {69.0, −72.1, −73.1, −76.6} ppm]. Resonances assigned to HF impurity (a doublet) and free $CH_3CN$ (parentheses) were observed in the $^1H$ spectra [−40 °C: 6.16 ppm, $^1J(^1H-^{19}F)$ = 496 Hz (1.94 ppm, $^1J(^1H-^{13}C)$ = 131 Hz); −80 °C: 6.69 ppm, 487 Hz (1.26 ppm, $^1J(^1H-^{13}C)$ = 130 Hz); −84 °C: 7.19 ppm, $^1J(^1H-^{13}C)$ = 47 Hz (1.51 ppm, $^1J(^1H-^{13}C)$ = 136 Hz)]. [g] Unreacted $CH_3C^{15}N$ was also observed in the $^{13}C\{^1H\}$ (117.50 [CN] and 0.86 [$CH_3$] ppm) and $^{15}N$ (−138.3 ppm) spectra.

(596 $cm^{-1}$)[23] and is shifted to higher frequency than in $OsO_3F_3^-$ (573 $cm^{-1}$),[3] consistent with a neutral species. The out-of-phase stretching mode is intermediate within the span of asymmetric Os−F stretching modes observed for $(OsO_3F_2)_\infty$ (610 $cm^{-1}$)[23] and $OsO_3F_3^-$ (504 $cm^{-1}$).[3] Its intermediacy is consistent with that observed for the Os−O stretching modes (vide supra). The Os---N stretching band at 204 $cm^{-1}$ is weak and intermediate with respect to the M---N stretching frequencies of other $CH_3CN$ adducts such as $TcO_2F_3(NCCH_3)$ (217 $cm^{-1}$),[9] $[ReO_2F_2(CH_3CN)_2][SbF_6]$ (264 $cm^{-1}$),[32] and $ReO_2F_3(NCCH_3)$ (252 $cm^{-1}$).[8]

The $\nu$(CN) stretching band of the coordinated $CH_3CN$ molecule (2332 $cm^{-1}$) occurs at significantly higher frequency than that of free $CH_3CN$ (2248 $cm^{-1}$). The high-frequency shift is consistent with donation of electron density by the nitrogen ligand atom to osmium, which strengthens the C−N bond as a result of nitrogen rehybridization to give more s character to the CN $\sigma$-bond.[41] Thus, backbonding from Os(VIII) into the $\pi^*$ orbitals of the CN group is not important because it would lead to a decrease in $\Delta\nu$(CN). The calculated complexation shifts at the SVWN ($\Delta\nu$(CN), 75 $cm^{-1}$) and B3LYP ($\Delta\nu$(CN), 59 $cm^{-1}$) levels are in good agreement with the experimental complexation shift ($\Delta\nu$(CN), 84 $cm^{-1}$). The bands at 952 and 956 $cm^{-1}$ are assigned to $\nu$(CC) of coordinated $CH_3CN$ at the B3LYP level, which weakly in-phase and out-of-phase couple with $\nu(OsO_3)$ at the SVWN level (vide supra). The $\nu$(CC) band shifts to higher frequency at the SVWN and B3LYP levels upon coordination (exptl., $\Delta\nu$(CC), 34 $cm^{-1}$; calcd., $\Delta\nu$(CC), 40 and 19 $cm^{-1}$, respectively), indicating a strengthened C−C bond. The experimental complexation shifts for $\nu$(CN) and $\nu$(CC), and their trends are similar to those of $TcO_2F_3(NCCH_3)$ ($\Delta\nu$(CN), 49; $\Delta\nu$(CC), 18 $cm^{-1}$)[9] and $ReO_2F_3(NCCH_3)$ ($\Delta\nu$(CN), 75; $\Delta\nu$(CC), 22 $cm^{-1}$),[8] suggesting similar Lewis acid strengths for monomeric $OsO_3F_2$, $TcO_2F_3$, and $ReO_2F_3$. The C−H bonds are little affected by coordination to osmium, with the experimental and calculated $CH_3$ group frequencies showing no significant complexation shifts.

There are four modes associated with the in-plane and out-of-plane $\delta$(NCC) bending modes (relative to the [O2, O3, Os, F1, N]-plane). The $\delta(NCC)_{ip}$ bend is observed at 415 $cm^{-1}$, while the $\delta(NCC)_{oop}$ bend is predicted to occur at higher frequency, but could not be observed. The remaining out-of-plane and in-plane bending modes are both weakly coupled to O−Os−O and F−Os−F bends to give bands at 277 and 326 $cm^{-1}$, respectively. The in-plane (232 $cm^{-1}$) and out-of-plane (216 $cm^{-1}$) $\delta$(Os---NC) bending modes are to higher frequency than the Re---NC bending modes in $ReO_2F_3(NCCH_3)$ (174 and 154 $cm^{-1}$).[8]

**NMR Spectroscopy.** Table 4 lists the $^1H$, $^{13}C$, $^{15}N$, and $^{19}F$ NMR parameters for *fac*-$OsO_3F_2(^{14}NCCH_3)$ in $CH_3CN$ solvent (−40 °C), *fac*- and *mer*-$OsO_3F_2(^{14}NCCH_3)$ in $SO_2ClF$ solvent (−40 and −80 °C) and *fac*- and *mer*-$OsO_3F_2(^{15}NCCH_3)$ in $SO_2ClF$ solvent (−84 °C).

**(a) *fac*-$OsO_3F_2(NCCH_3)$.** The $^{19}F$ NMR spectrum of *fac*-$OsO_3F_2(^{14}NCCH_3)$ in $CH_3CN$ solvent at −40 °C consists of a singlet at −99.6 ppm, which is less shielded than the $^{19}F$ environment of $OsO_3F_3^-$ in $CH_3CN$ solvent (−116.8 ppm)[3] and considerably more shielded than both $^{19}F$ environments of *cis*-$OsO_2F_4$ (15.8 and 63.3 ppm) in anhydrous HF solvent.[39] This is consistent with a decrease in the number of strongly electron withdrawing fluorine ligands and the addition of the electron donating nitrogen and oxygen ligands. The $^{19}F$ chemical shift is intermediate with respect to those of $WOF_4(NCCH_3)$ (−68.5 ppm)[10] and $MoOF_4(NCCH_3)$ (−147.4 ppm)[7] recorded at −30 °C in $CH_3CN$. The $^1H$ NMR spectrum at −40 °C is a singlet corresponding to complexed $CH_3CN$ at 2.55 ppm ($^1J(^1H-^{13}C)$ = 126.1 Hz) which is shifted to higher frequency than the $^1H$ resonance of $CH_3CN$ solvent (2.06 ppm, $^1J(^1H-^{13}C)$ = 136.1 Hz), consistent with Lewis acid−base adduct formation. The complexation shift (0.49 ppm) is comparable to that of $TcO_2F_3(NCCH_3)$ in $CH_3CN$ solvent (0.37 ppm).[9]

The $^{19}F$ NMR spectrum of *fac*-$OsO_3F_2(^{14}NCCH_3)$ in $SO_2ClF$ solvent at −80 (−40) °C is a singlet at −97.6

(41) Purcell, K. F.; Drago, R. S. *J. Am. Chem. Soc.* **1966**, *88*, 919–924.

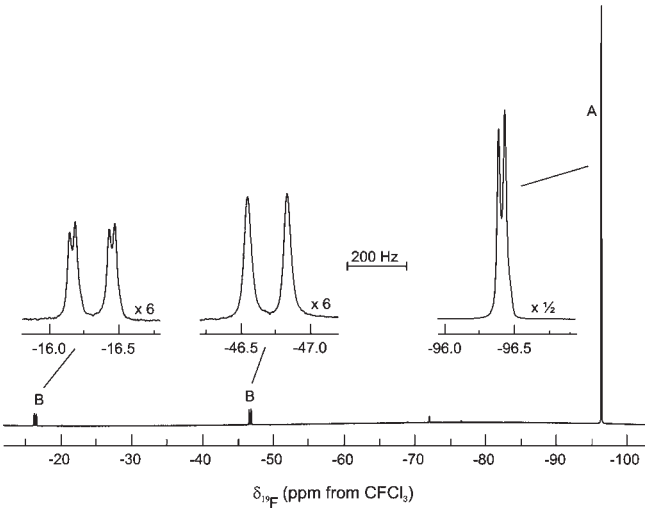


**Figure 3.** $^{19}F$ NMR spectra (470.409 MHz) of $^{15}N$-enriched *fac*-$OsO_3F_2(NCCH_3)$ (A) and *mer*-$OsO_3F_2(NCCH_3)$ (B) in $SO_2ClF$ solvent at −80 °C.

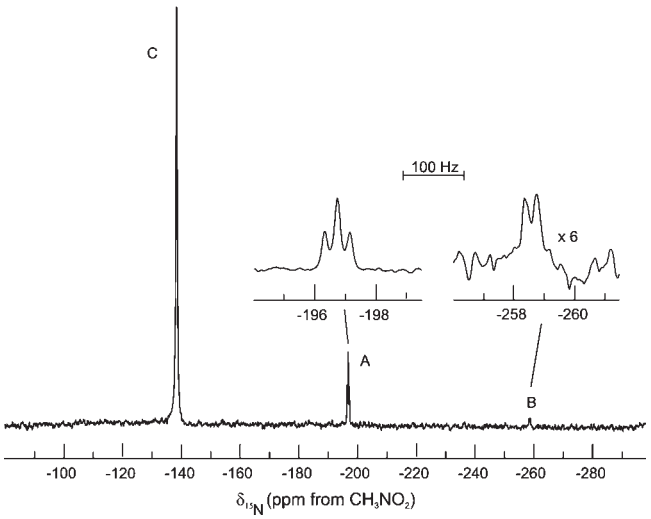


**Figure 4.** $^{15}N$ NMR spectra (50.693 MHz) of $^{15}N$-enriched *fac*-$OsO_3F_2(NCCH_3)$ (A), *mer*-$OsO_3F_2(NCCH_3)$ (B), and free $CH_3CN$ (C) in $SO_2ClF$ solvent at −80 °C.

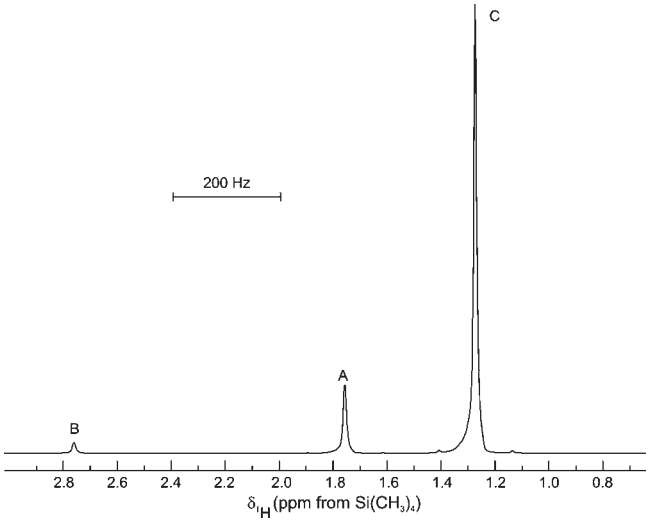


**Figure 5.** $^{1}H$ NMR spectra (500.138 MHz) of $^{15}N$-enriched *fac*-$OsO_3F_2(NCCH_3)$ (A), *mer*-$OsO_3F_2(NCCH_3)$ (B), and free $CH_3CN$ (C) in $SO_2ClF$ solvent at −80 °C.

(−93.6) ppm with $^{187}Os$ ($I$ = ½; natural abundance, 1.64%) satellites corresponding to $^1J(^{187}Os-^{19}F)$ = 41.2 Hz. The $^{187}Os-^{19}F$ coupling constant is greater than that observed for the $OsO_3F_3^-$ anion (32 Hz),[3] and is consistent with greater Os−F bond covalency in the neutral adduct, and is similar to one of the two $^1J(^{187}Os-^{19}F)$ couplings observed for *cis*-$OsO_2F_4$ (35.1 and 59.4 Hz).[39] In the latter case, the smaller coupling constant was tentatively assigned to $^1J(^{187}Os-^{19}F_a)$ where the fluorine ligands are trans to one another, and the larger coupling was assigned to $^1J(^{187}Os-^{19}F_e)$, where the fluorine ligands are trans to oxygen ligands. The F atoms are trans to O atoms for both $OsO_3F_3^-$ and $OsO_3F_2(NCCH_3)$, suggesting that the $^1J(^{187}Os-^{19}F)$ coupling and $^{19}F$ chemical shift assignments for *cis*-$OsO_2F_4$ should be interchanged.[42] Smaller $^1J(M-^{19}F)$ coupling constants for fluorine trans to oxygen relative to those for fluorine trans to fluorine have also been reported for $WO_2F_4^{2-}$ [43] and $TcO_2F_4^-$.[9] A $^{15}N$-enriched sample of *fac*-$OsO_3F_2(^{15}NCCH_3)$ in $SO_2ClF$ solvent resulted in splitting of the *fac*-$OsO_3F_2(^{15}NCCH_3)$ $^{19}F$ resonance at −96.8 ppm into a doublet ($^2J(^{19}F-^{15}N)$, 21.4 Hz, Figure 3), confirming that a single $CH_3CN$ molecule is coordinated to osmium and that both fluorine ligands are chemically equivalent.

The $^{15}N$ NMR resonance of *fac*-$OsO_3F_2(^{15}NCCH_3)$ (Figure 4) at −197.3 ppm is a triplet ($^2J(^{15}N-^{19}F)$ = 21.4 Hz) which is consistent with splitting of the $^{15}N$ resonance by coupling to two chemically equivalent fluorine nuclei. The $^{15}N$ resonance of the complexed $CH_3C^{15}N$ ligand is shifted by 59.0 ppm to lower frequency when compared with that of free $CH_3C^{15}N$ (−138.3 ppm) in $SO_2ClF$ solvent.

The $^{1}H$ NMR spectra of *fac*-$OsO_3F_2(^{14}NCCH_3)$ and *fac*-$OsO_3F_2(^{15}NCCH_3)$ (Figure 5) recorded in $SO_2ClF$ solvent at −80 (−40) °C are singlets at 1.76 (2.66) ppm ($^1J(^1H-^{13}C)$, 139.5 (137.9) Hz) and 2.02 ppm ($^1J(^1H-^{13}C)$, 139.8 Hz), respectively. The $^{1}H$ complexation shifts for the $^{14}N$ (0.50 ppm) and $^{15}N$ (0.51 ppm) isotopomers are comparable to that observed for $ReO_2F_3(NCCH_3)$ in $SO_2ClF$ (0.59 ppm).[8] A singlet was observed at 2.24 ppm in the $^{13}C\{^1H\}$ NMR spectrum of *fac*-$OsO_3F_2(^{15}NCCH_3)$ (−80 °C) which resulted from the methyl carbon of the coordinated $CH_3CN$ ligand, representing a 1.59 ppm complexation shift relative to free $CH_3CN$ (0.65 ppm), also observed in the same sample. The $^{13}C$ resonances of complexed $CH_3CN$ could not be observed in $CH_3CN$ solvent presumably because they overlap with the solvent peaks.

**(b) *mer*-$OsO_3F_2(NCCH_3)$.** The $^{19}F$ NMR spectra of *mer*-$OsO_3F_2(^{14}NCCH_3)$ at −40 [−80] °C in $SO_2ClF$ solvent consisted of two weak doublets assigned to the equatorial (−13.1 [−15.4] ppm) and axial (−44.4 [−46.1]

(42) The low-frequency $^{19}F$ resonance of *cis*-$OsO_2F_4$ (15.8 ppm; $^1J(^{187}Os-^{19}F)$, 35.1 Hz) should be reassigned to the two equatorial fluorine ligands trans to oxygen, and the high-frequency $^{19}F$ resonance (63.3 ppm $^1J(^{187}Os-^{19}F)$, 59.4 Hz) should be reassigned to the mutually trans axial fluorine ligands. The reassignment is now consistent with the range of $^1J(^{187}Os-^{19}F)$ coupling constants for fluorine trans to oxygen in other Os(VIII) oxide fluorides, namely, *cis*-$OsO_2F_4$, *fac*-$OsO_3F_2(NCCH_3)$, and *fac*-$OsO_3F_3^-$.

(43) Buslaev, Y. A.; Petrosyants, S. P. *J. Struct. Chem.* **1969**, *10*, 983–985; *Zh Strukt. Khim.* **1969**, *10*, 1105−1107.

ppm) fluorine environments with $^2J(^{19}F_1-^{19}F_2)$ = 134.3 [135.0] Hz, which is similar to the two-bond fluorine-fluorine coupling constant of *cis*-$OsO_2F_4$ (138.3 Hz).[39] The $^{19}F$ NMR spectrum of *mer*-$OsO_3F_2(^{15}NCCH_3)$, recorded at −84 °C, consisted of a weak doublet of doublets at −17.9 ppm assigned to $F_1$ and a weak doublet, of equal intensity, at −48.0 ppm assigned to $F_2$ with $^2J(^{19}F_1-^{19}F_2)$ = 134.3 Hz and $^2J(^{15}N-^{19}F_1)$ = 18.3 Hz (Figure 3). The $^2J(^{15}N-^{19}F_2)$ coupling was not resolved.

The $^{15}N$ NMR spectrum of the $^{15}N$ enriched *mer*-$OsO_3F_2(NCCH_3)$ (Figure 4) consisted of a doublet at −258.6 ppm which resulted from coupling to the equatorial fluorine ($^2J(^{15}N-^{19}F_1)$ = 18.3 Hz); however, as in the $^{19}F$ NMR spectrum, the $^2J(^{15}N-^{19}F_2)$ coupling to the axial fluorine was not resolved.

Two-bond coupling constants are known to have a bond angle dependence, with the coupling constant increasing with increasing bond angle so that a *trans*-$^2J$ coupling is generally larger in magnitude than a *cis*-$^2J$ coupling.[44] The $^2J(^{15}N-^{19}F_1)$ coupling constant is therefore expected to be larger than $^2J(^{15}N-^{19}F_2)$. The only splitting observed on the resonance at −17.9 ppm has therefore been assigned to $^2J(^{15}N-^{19}F_1)$ assuming that the $^2J(^{15}N-^{19}F_2)$ coupling on the resonance at −48.0 ppm is smaller and therefore could not be resolved.

The $^1H$ NMR spectrum recorded in $SO_2ClF$ (Figure 5) is a singlet at 3.12 ppm (−40 °C, $^1J(^1H-^{13}C)$ = 142.8 Hz) and at 3.04 ppm (−80 °C, $^1J(^1H-^{13}C)$ = 140.4 Hz). The complexation shift (av., 1.53 ppm) is significantly greater than that observed for *fac*-$OsO_3F_2(NCCH_3)$ (av., 0.51 ppm), in accordance with the shorter calculated Os---N bond length (see Calculated Geometries). The $^{13}C\{^1H\}$ NMR spectrum consists of a singlet at 2.39 ppm for the methyl carbon of the coordinated $CH_3CN$ ligand; however, a $^{13}C$ signal could not be observed for the cyano carbon of the natural abundance sample at either temperature.

**Reaction Pathways Leading to *fac*- and *mer*-$OsO_3F_2(NCCH_3)$.** In addition to *fac*-$OsO_3F_2(NCCH_3)$ (Structure I), two other $OsO_3F_2(NCCH_3)$ isomers are possible in which the oxygen ligands have *mer*-arrangements. These meridional isomers are distinguished by coordination of $CH_3CN$ trans to a F atom (*mer*-$OsO_3F_2(NCCH_3)$, Structure II) and by coordination of $CH_3CN$ trans to an O atom (*mer′*-$OsO_3F_2(NCCH_3)$, Structure III). Solution NMR studies and the solid-state Raman spectrum and a single-crystal X-ray structure reveal that only the *fac*-isomer is observed in the solid state and in $CH_3CN$ solution, whereas a mixture of *fac*- and *mer*-$OsO_3F_2(NCCH_3)$ is observed in $SO_2ClF$ solvent where the *fac*-isomer is strongly favored over the *mer*-isomer. No experimental evidence for the *mer′*-isomer was obtained. The ensuing discussion proposes likely pathways that lead to the *mer*- and *fac*-isomers and account for the absence of the *mer′*-isomer.

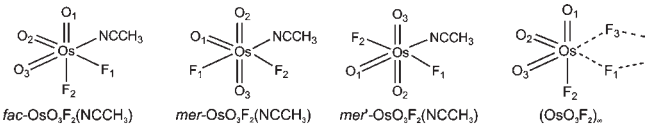


I II III IV

In the solid state, $(OsO_3F_2)_\infty$ is a fluorine-bridged polymer in which the Os atoms are pseudo-octahedrally coordinated, having a *fac*-trioxo arrangement and two bridging F atoms and one terminal F atom that are trans to O atoms (Structure IV). The Os---$F_{1,3}$ bridge bonds can be regarded as half bonds relative to the terminal Os−$F_2$ bond of the $(OsO_3F_2)_\infty$ polymer. Thus, the fluorine bridge ligand is the only viable leaving group for displacement by $CH_3CN$.[23] When $(OsO_3F_2)_\infty$ is dissolved in $CH_3CN$, the direction of solvent attack must be along a pseudo 3-fold axis along which a $d_{t_{2g}}$ metal orbital points. The preferred face for attack will be the least sterically hindered face of the pseudo-octahedron which is composed of two bridging fluorine ligands and an oxygen ligand, and leads exclusively to the *fac*-isomer (Scheme 1a). Dissociation of *fac*-$OsO_3F_2(NCCH_3)$ to the trigonal bipyramidal *cis*-$OsO_3F_2$ intermediate is suppressed in $CH_3CN$ solvent so that isomerization to *mer*-$OsO_3F_2(NCCH_3)$ is prevented (Scheme 1b). Isomerization occurs, however, when $OsO_3F_2(NCCH_3)$ is formed in $SO_2ClF$ solvent because the equilibrium leading to *cis*-$OsO_3F_2$ ($C_s$) is no longer suppressed, allowing $CH_3CN$ to recombine by coordination in the trigonal plane of *cis*-$OsO_3F_2$ at (a) the sterically least congested sites between the equatorial fluorine ligand and an oxygen ligand to give *fac*-$OsO_3F_2(NCCH_3)$ (Scheme 1c) or at (b) the sterically most congested and least favored site between two oxygen ligands to give *mer*-$OsO_3F_2(NCCH_3)$ (Scheme 1d). Thus, the pathway that leads to *fac*-$OsO_3F_2(NCCH_3)$ in $SO_2ClF$ is twice as likely as that which leads to *mer*-$OsO_3F_2(NCCH_3)$. The experimental isomer ratios are not statistical (*fac*/*mer* = 2), but are significantly skewed toward the *fac*-isomer because of steric and electronic effects which also favor the *fac*-isomer. In $SO_2ClF$ solvent, a plausible path from *fac*-$OsO_3F_2(NCCH_3)$ and *mer*-$OsO_3F_2(NCCH_3)$ to *mer′*-$OsO_3F_2(NCCH_3)$ commences with dissociation of *fac*- or *mer*-$OsO_3F_2(NCCH_3)$ to *cis*-$OsO_3F_2$ ($C_s$) followed by intramolecular ligand exchange by means of Berry pseudorotation to give the *cis,trans*-$OsO_3F_2$ ($C_{2v}$) and *eq*-$OsO_3F_2$ ($D_{3h}$) intermediates (Scheme 1e). Recombination by $CH_3CN$ coordination to *cis,trans*-$OsO_3F_2$ in the trigonal plane between one of the F atoms and the O atom affords *mer*-$OsO_3F_2(NCCH_3)$ (Scheme 1f) whereas coordination between the two F atoms affords *mer′*-$OsO_3F_2(NCCH_3)$ (Scheme 1g), which is sterically more favorable, but statistically less favorable. The calculated relative stabilities of *cis*-$OsO_3F_2$ ($C_s$) and *eq*-$OsO_3F_2$ ($D_{3h}$) are similar with *cis*-$OsO_3F_2$ ($C_s$) being slightly more stable (5.7 kJ $mol^{-1}$) at the B3LYP level of theory and *eq*-$OsO_3F_2$ ($D_{3h}$) being slightly more stable (3.1 kJ $mol^{-1}$) at the SVWN level of theory. Attempts to optimize the structure of the *cis, trans*-$OsO_3F_2$ ($C_{2v}$) intermediate failed at both the SVWN and B3LYP levels of theory, yielding only *eq*-$OsO_3F_2$ ($D_{3h}$) as the optimized structure. To ensure failure to optimize the *cis*-, *trans*-$OsO_3F_2$ ($C_{2v}$) intermediate was not basis set dependent, a further attempt was made at the B3LYP level using the aug-cc-pVTZ(-PP) basis set for Os. Once again the optimization only gave the *eq*-$OsO_3F_2$ ($D_{3h}$) geometry. Thus, there is apparently no pathway that converts *cis*-$OsO_3F_2$ to *cis, trans*-$OsO_3F_2$ by means of Berry pseudorotation. Although the stabilities of *cis*-$OsO_3F_2$ and *eq*-$OsO_3F_2$ are very similar, the non-existence of the *cis, trans*-$OsO_3F_2$ intermediate renders isomerization pathways f−h in Scheme 1 untenable. Alternative rearrangements

(44) Mason, J. *Multinuclear NMR*, 2nd ed.; Plenum Press: New York, 1987.

**Scheme 1.** Reaction Pathways That Account for the Formation of the Experimentally Observed *fac*- and *mer*-$OsO_3F_2(NCCH_3)$ Isomers and the Absence of *mer*′-$OsO_3F_2(NCCH_3)$

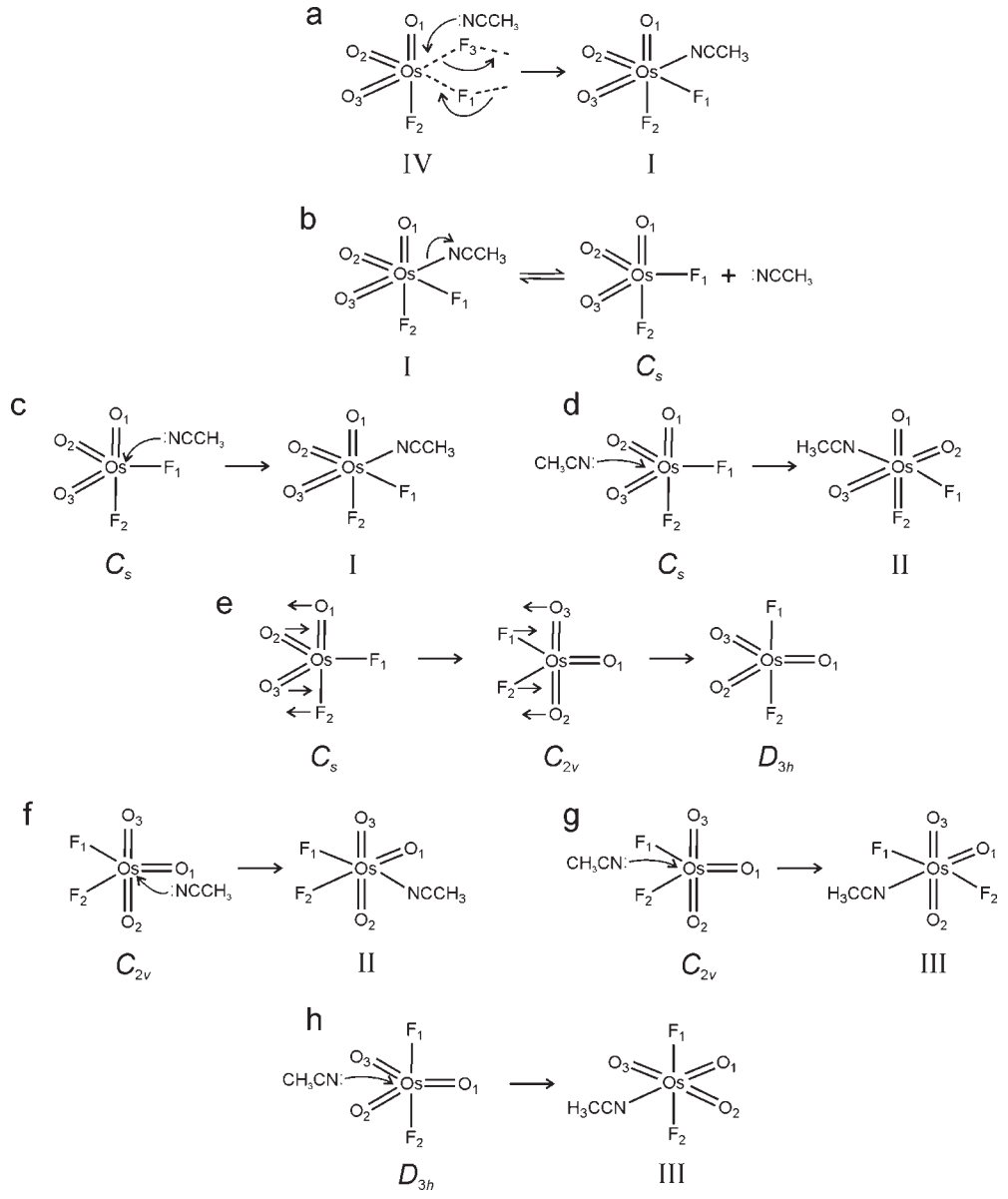


by dissociative mechanisms would be predicated on the dissociation of the *cis*-$OsO_3F_2$ to $OsO_3F^+$ and $F^-$, which; however, would present a formidable barrier, with gas-phase dissociation energies of 948 (SVWN) and 872 (B3LYP) kJ $mol^{-1}$. Moreover, a dissociative mechanism would not be viable under the present basic solvent conditions because $OsO_3F^+$ can only be generated by fluoride ion abstraction using strong Lewis acid fluoride ion acceptors.[24]

The reaction pathways in Scheme 1 suggest that the most abundant isomer should be *fac*-$OsO_3F_2(NCCH_3)$, consistent with the $CH_3CN$ solution NMR studies and isolation of this isomer from $CH_3CN$ solution. The weaker resonances in $SO_2ClF$ solution have a splitting pattern and abundance consistent with *mer*-$OsO_3F_2(NCCH_3)$. The above considerations account for why the *fac*-isomer was always present in significantly higher concentration than the *mer*-isomer in $SO_2ClF$ solution and why *mer*′-$OsO_3F_2(NCCH_3)$ is not observed.

## Computational Results

The calculated geometries of *fac*- and *mer*-$OsO_3F_2(NCCH_3)$ (Figure 6) optimized under $C_1$ symmetry at the SVWN [B3LYP] levels of theory and resulted in stationary points with all frequencies real. The starting geometry for *fac*-$OsO_3F_2(NCCH_3)$ was the crystallographic geometry, and the starting geometry for *mer*-$OsO_3F_2(NCCH_3)$ was obtained by interchanging the positions of one oxygen and one fluorine atom in the optimized geometry of *fac*-$OsO_3F_2(NCCH_3)$. The energy-minimized geometries (Table 2 and Supporting Information, Figure S3) and vibrational frequencies (Table 3) of $CH_3CN$ ($C_{3v}$) and *cis*- $OsO_2F_4$ ($C_{2v}$)[23] were also calculated to serve as benchmarks and for comparison with *fac*- and *mer*-$OsO_3F_2(NCCH_3)$.

**(a) Calculated Geometries. (i) *fac*-$OsO_3F_2(NCCH_3)$.** The calculated geometries of *fac*-$OsO_3F_2(NCCH_3)$ (Figure 6a) are in good agreement with the experimental geometry. Overall, the B3LYP values provide slightly

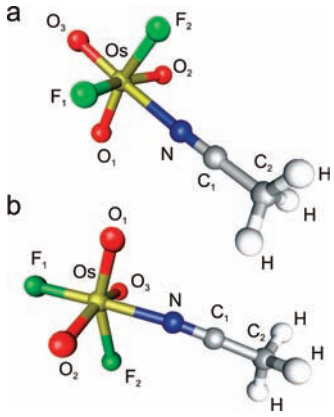


**Figure 6.** Calculated SVWN/SDDall gas-phase geometries for (a) *fac*-$OsO_3F_2(NCCH_3)$ ($C_1$), (b) *mer*-$OsO_3F_2(NCCH_3)$ ($C_1$).

better agreement with the experimental bond lengths, although the Os---N bond length (2.260 [2.386] Å) is overestimated when compared with the experimental value (2.205(3) Å). The Os−O bond lengths (1.727, 1,712 [1.701, 1.687] Å) are in good agreement with the experimental values (1.707(2), 1.704(2), 1.699(2) Å); however, the calculations overestimate the bond length differences between bonds that are trans to F and those that are trans to O. The Os---F bond lengths (1.922 [1.922] Å) are slightly underestimated when compared with the experimental values (1.939(2) Å). The experimental bond angles are all well reproduced by both methods, the largest discrepancy being the Os---N−C bond angle, which is calculated to be 170.5 [173.7]° instead of the almost linear experimental value of 178.4(2)°. The deviation from linearity for the calculated structure is likely a result of the $CH_3CN$ ligand being repelled by the Os−O double bond domain toward the Os−F single bond domain. The near-linear Os---N−C bond angle in the crystal structure is attributed to crystal packing because this angle is very deformable as suggested by the low calculated Os---N−C bending frequencies (214 and 217 $cm^{-1}$). The N−C and C−C bond lengths of the adducted $CH_3CN$ molecule are slightly shorter than those predicted for the free $CH_3CN$ molecule, in agreement with experiment.

**(ii) *mer*-$OsO_3F_2(NCCH_3)$.** The energy-minimized geometry of *mer*-$OsO_3F_2(NCCH_3)$ (Figure 6b) has a pseudo-octahedral osmium coordination sphere in which the nitrogen atom of $CH_3CN$ is coordinated trans to a fluorine atom (Os−N, 2.114 [2.175] Å). The $O_2$ and $O_3$ atoms are equidistant from the osmium atom (1.760 [1.736] Å) with a somewhat shorter Os−$O_1$ bond length (1.728 [1.705] Å). The longer Os−$O_{2,3}$ bond lengths result from the mutual trans influences of the oxygen ligands, whereas the shorter Os−$O_1$ bond length results because $O_1$ is trans to a fluorine ligand, $F_2$. The $F_1$ atom is trans to the $CH_3CN$ ligand, resulting in a Os−$F_1$ bond length (1.863 [1.857] Å) that is shorter than the Os−$F_2$ bond length (1.968 [1.972] Å). The longer Os−$F_2$ bond length results from the greater trans influence of $O_1$ when compared with that of the $CH_3CN$ ligand. The N---Os−$O_{2,3}$ bond angles are equal (91.0 [88.9]°) and more open than the N---Os−$O_1$ (84.2 [83.1]°) and N---Os−$F_2$ (73.4 [75.4]°) bond angles.

The N−C and C−C bond lengths of the adducted $CH_3CN$ molecule are slightly shorter than those calculated for the free $CH_3CN$ molecule, in accordance with the relatively short Os---N bond length (2.114 [2.175] Å), and are comparable to those of the *fac*-isomer (vide supra).

**(b) Charges, Valencies, and Bond Orders.** The NBO[45−48] analyses were carried out for the SVWN- and B3LYP-optimized gas-phase geometries of *fac*-$OsO_3F_2(NCCH_3)$, *mer*-$OsO_3F_2(NCCH_3)$, and $CH_3CN$. The NBO results are given in Supporting Information, Table S3. The SVWN and B3LYP results are similar for the experimentally observed *fac*- and *mer*-$OsO_3F_2(NCCH_3)$ isomers; therefore, only the SVWN results are referred to in the ensuing discussion.

The NBO analyses give natural population analysis (NPA) charges for Os of 1.83 and 1.76 in *fac*- and *mer*-$OsO_3F_2(NCCH_3)$, respectively. The NPA charges of the oxygen, fluorine, and nitrogen ligand atoms are negative with charges that are somewhat less than −0.50, indicating that the bonds formed with the osmium atom are polar covalent.

The Os−O bond orders (fac, 0.84 and mer, 0.81) are approximately twice the Os−F bond order (fac 0.42 and 0.42 and mer 0.50 and 0.40). The Os−N bond orders indicate that the Os---N bonds have significant covalent character. The Os−N bond order of the *fac*-isomer (0.29) is significantly less than the Os−N bond order of the *mer*-$OsO_3F_2(NCCH_3)$ isomer (0.40), indicating that the latter Os−N bond is expected to be stronger than that of the *fac*-$OsO_3F_2(NCCH_3)$ isomer, consistent with its shorter calculated bond length (vide supra) and coordination of the $CH_3CN$ ligand trans to a fluorine ligand.

The charges on the N atoms of the adducted $CH_3CN$ ligands (fac, −0.41 and mer, −0.37) are more negative than that of the free ligand (−0.31), whereas the charges on the $C_1$ atoms (fac, 0.49 and mer, 0.53) are more positive than that of $CH_3CN$ (0.28). The C−N bond orders (1.76 and 1.74, respectively) are less than that of the free ligand (1.84). The charge differences and C−N bond orders indicate that the adducted ligand is polarized by the electronegative Os(VIII) center and that significant electron density has migrated from the formal C−N triple bond to the N atom. As expected, the charges, valencies, and bond orders of the $CH_3$ group do not change significantly upon adduct formation.

**(c) Calculated Frequencies.** The vibrational frequencies, intensities, and assignments for *fac*- and *mer*-$OsO_3F_2(NCCH_3)$ were calculated at the SVWN and B3LYP levels (Supporting Information, Table S4) and confirm that the assignments of the experimental vibrational frequencies are consistent with *fac*-$OsO_3F_2(NCCH_3)$ (see Raman Spectroscopy).

(45) Reed, A. E.; Weinstock, R. B.; Weinhold, F. *J. Chem. Phys.* **1985**, *83*, 735–746.
(46) Glendening, E. D.; Reed, A. E.; Carpenter, J. E.; Weinhold, F. In *NBO*, Version 3.1; Gaussian Inc.: Pittsburgh, PA, 1990.
(47) Reed, A. E.; Curtiss, L. A.; Weinhold, F. *Chem. Rev.* **1998**, *88*, 899–926.
(48) Glendening, E. D.; Badenhoop, J. K.; Reed, A. E.; Carpenter, J. E.; Bohmann, C. M.; Morales, C. M.; Weinhold, F. In *NBO*, Version 5.0; Theoretical Chemical Institute, University of Wisconsin: Madison WI, 2001.

The *fac*- and *mer*-isomers cannot be differentiated based solely on the $CH_3CN$ ligand frequencies. The calculated frequencies between 1040 and 3072 $cm^{-1}$ are assigned to the adducted $CH_3CN$ molecule, are comparable for the *mer*- and *fac*-isomers, and are in good agreement with the experimental frequencies of the *fac*-isomer.

The presence of *mer*-$OsO_3F_2(NCCH_3)$ is discounted for the following reasons: (1) The calculated $\nu$(CC) and $\nu$(OsO) stretching frequencies of *fac*- and *mer*-$OsO_3F_2(NCCH_3)$ occur between 949−988 $cm^{-1}$ and 888−1002 $cm^{-1}$, respectively, whereas the experimental $\nu$(CC) and $\nu$(OsO) stretches occur between 910−956 $cm^{-1}$. The frequency range of the *fac*-isomer is significantly narrower than that of the *mer*-isomer and more consistent with the experimental frequency range. (2) The bands associated with the Os−F stretches are coupled in the case of the *fac*-$OsO_3F_2(NCCH_3)$ isomer, giving rise to in-phase, $\nu(OsF_1) + \nu(OsF_2)$, and out-of-phase, $\nu(OsF_1) - \nu(OsF_2)$, modes with frequencies calculated at 564 and 624 $cm^{-1}$, respectively. In contrast, Os−F stretches of *mer*-$OsO_3F_2(NCCH_3)$ are not coupled, with $\nu(OsF_2)$ and $\nu(OsF_1)$ calculated at 531 and 663 $cm^{-1}$. When compared with the experimental $\nu$(OsF) stretching frequencies of the *fac*-isomer (529 and 598; $\Delta\nu$, 68 $cm^{-1}$), the calculated difference between the two $\nu$(OsF) modes of the *mer*-$OsO_3F_2(NCCH_3)$ isomer ($\Delta\nu$, 132 $cm^{-1}$) is much greater. Overall, the calculated frequencies of *fac*-$OsO_3F_2NCCH_3$) provide the best overall agreement with the experimental spectrum.

**(d) Relative Stabilities of *fac*-$OsO_3F_2(NCCH_3)$ and *mer*-$OsO_3F_2(NCCH_3)$.** The reaction enthalpies and Gibbs free energies were calculated for the conversion of *fac*-$OsO_3F_2(NCCH_3)$ to *mer*-$OsO_3F_2(NCCH_3)$ at the SVWN and B3LYP levels of theory at 298, 233, and 193 K (Supporting Information, Table S5). The calculated enthalpy changes demonstrate that the *fac*-isomer is preferred over the *mer*-isomer by 114.4(1) (SVWN) and 121.2(3) (B3LYP) kJ $mol^{-1}$, which is consistent with the experimental findings. As expected for an isomerization, the $\Delta G$ values at the SVWN (−115.2 to −117.8 kJ $mol^{-1}$) and B3LYP levels (−122.6 to −123.4 kJ $mol^{-1}$) do not show a large entropy dependence with little variation in $\Delta G$ with temperature.

## Conclusions

Fluorine-19 NMR spectroscopy reveals that dissolution of $(OsO_3F_2)_\infty$ in $CH_3CN$ solvent exclusively yields *fac*-$OsO_3F_2(NCCH_3)$, and single-crystal X-ray diffraction has shown that crystallization from $CH_3CN$ solvent at −45 °C yields *fac*-$OsO_3F_2(NCCH_3)\cdot 2CH_3CN$. The $F_2O_3OsN$-moiety in the X-ray crystal structure of *fac*-$OsO_3F_2(NCCH_3)\cdot 2CH_3CN$ is pseudo-octahedral with the three oxygen ligands in a facial arrangement and the $CH_3CN$ ligand nitrogen coordinated to osmium. The $CH_3CN$ solvent molecules in the crystal lattice can be removed under dynamic vacuum at −40 °C to yield unsolvated *fac*-$OsO_3F_2(NCCH_3)$. The *fac*- and *mer*- isomers of $OsO_3F_2(NCCH_3)$ were observed in $SO_2ClF$ solvent and confirmed by their spin−spin coupling patterns in their low-temperature $^{19}F$ and $^{15}N$ NMR spectra. The Raman spectra of the solids isolated from $CH_3CN$ and $SO_2ClF$ solutions are identical and are attributed to *fac*-$OsO_3F_2(NCCH_3)$. The vibrational assignments of *fac*-$OsO_3F_2(NCCH_3)$ were confirmed by the calculated vibrational frequencies which show better agreement with the experimental results than the calculated values for *mer*-$OsO_3F_2(NCCH_3)$. Thermochemical calculations are consistent with experiment, showing that the *fac*-isomer is favored over the *mer*-isomer by about 118 kJ $mol^{-1}$. Quantum-chemical calculations and the proposed reaction pathways account for why *fac*-$OsO_3F_2(NCCH_3)$ is observed exclusively in $CH_3CN$ solvent and why a mixture of *fac*- and *mer*-$OsO_3F_2(NCCH_3)$ isomers is observed in $SO_2ClF$, with the *fac*-isomer dominating in the latter case. The proposed reaction pathways also account for the absence of *mer*′-$OsO_3F_2(NCCH_3)$.

## Experimental Section

**Apparatus and Materials.** Manipulations involving air-sensitive materials were carried out under anhydrous conditions as previously described.[31] All preparative work was carried out in vessels constructed from ¼-in. o.d. lengths of FEP tubing. The tubing was heat-sealed at one end and connected through a 45° SAE flare to a Kel-F valve. Reaction vessels were dried on a Pyrex glass vacuum line and then transferred to a metal vacuum line where they were passivated with $F_2$ for several hours, refilled with dry $N_2$, and placed in a drybox until used. All vacuum line connections were made by use of ¼-in. 316 stainless steel Swagelok Ultratorr unions fitted with Viton O-rings. Osmium trioxide difluoride, $(OsO_3F_2)_\infty$, was synthesized by reaction of $OsO_4$ (Koch-Light, 99.9%) with $ClF_3$ as previously described.[22] Acetonitrile (Caledon HPLC grade) was purified according to the literature procedure[49] and $CH_3C^{15}N$ (Isotec, > 99%) was dried over $CaH_2$ powder (Aldrich, 90−95%) for several days followed by vacuum distillation into a dry glass vessel and storage under dry $N_2$ until used.

**Syntheses of *fac*-$OsO_3F_2(NCCH_3)\cdot 2CH_3CN$ and *fac*-$OsO_3F_2(NCCH_3)$.** In a typical synthesis, a fluorine passivated FEP tube was loaded inside a drybox with 0.0545 g (0.1973 mmol) of orange $(OsO_3F_2)_\infty$ using a Teflon scoop fitted to a 1/16 in. Ni rod.[23] The reaction vessel was then transferred to a glass vacuum line, and about 0.1 mL of $CH_3CN$ was condensed into the tube at −196 °C. Upon warming to −40 °C with agitation, a yellow-brown precipitate and orange supernatant resulted. Excess $CH_3CN$ was removed under dynamic vacuum at −40 °C, initially yielding *fac*-$OsO_3F_2(NCCH_3)\cdot 2CH_3CN$ which was followed by the formation of *fac*-$OsO_3F_2(NCCH_3)$ upon further pumping at −40 °C. Both compounds were isolated as yellow-brown solids. The sample composition was monitored by Raman spectroscopy (Supporting Information, Table S1).

**Nuclear Magnetic Resonance Spectroscopy. (a) NMR Sample Preparation.** Samples for NMR spectroscopy were prepared in 4-mm o.d. FEP tubes that were flared and fitted with Kel-F valves. A sample of $OsO_3F_2(NCCH_3)$ was prepared by condensing ca. 0.3 mL of $CH_3CN$ onto 0.0305 g (0.1104 mmol) of $(OsO_3F_2)_\infty$ contained in a 4-mm NMR tube at −196 °C. The sample was warmed to −40 °C and allowed to react. NMR samples containing *fac*-$OsO_3F_2(NCCH_3)$ and *mer*-$OsO_3F_2(NCCH_3)$ [$OsO_3F_2(^{15}NCCH_3)$] in $SO_2ClF$ solvent were prepared by condensing ca. 0.02 mL of $CH_3CN$ [0.0065 g, 0.15 mmol of $CH_3C^{15}N$] onto 0.0335 g, 0.129 mmol [0.0208 g, 0.0753 mmol] of $(OsO_3F_2)_\infty$ in a 4-mm FEP tube at −196 °C. After melting $CH_3CN$ at −40 °C and initial mixing, ca. 0.3 mL of $SO_2ClF$ was condensed onto the mixture at −196 °C. The NMR samples were then heat-sealed under dynamic vacuum and stored at −196 °C until their NMR spectra could be obtained. Samples were dissolved just prior to data acquisition at or below the temperature used to record their spectra. Spectra were recorded by

(49) Winfield, J. M. *J. Fluorine Chem.* **1984**, *25*, 91–98.

inserting the 4-mm o.d. FEP sample tubes into 5-mm o.d. thin-wall precision glass NMR tubes (Wilmad).

**(b) NMR Instrumentation and Spectral Acquisitions.** Proton, $^{13}C$, $^{15}N$, and $^{19}F$ nuclear magnetic resonance spectra were recorded unlocked (field drift ca. 0.1 Hz $h^{-1}$) on a Bruker DRX-500 spectrometer equipped with an 11.744-T cryomagnet. The NMR probe was cooled using a nitrogen flow and variable-temperature controller (BVT 3000).

The $^{19}F$ ($^{1}H$) NMR spectra were acquired using a 5-mm combination $^{1}H/^{19}F$ probe operating at 470.592 (500.138) MHz. The spectra were recorded in 64 (32) K memories with spectral width settings of 160 (20) kHz and acquisition times of 0.33 (0.82) s, and were zero-filled to 64 (32) K, yielding data point resolutions of 1.52 (0.61) Hz/data point. Relaxation delays of 0.05 (0.5) s were applied and 1400 (440) transients were accumulated.

The $^{13}C$ ($^{15}N$) NMR spectra were acquired using a 5-mm broad-band inverse probe operating at 125.755 (50.693) MHz. The spectra were recorded in 32 K memories with spectral width settings of 24 (50) kHz and acquisition times of 0.33 (0.17) s, and were zero-filled to 16 (16) K, yielding data point resolutions of 1.52 (3.05) Hz/data point. Relaxation delays of 5.0 (5.0) s were applied, and 16 000 (153 000) transients were accumulated.

Pulse widths, corresponding to bulk magnetization tip angles of approximately 90°, were 2.5 ($^{1}H$), 5.0 ($^{13}C$), 12 ($^{15}N$), and 8.5 ($^{19}F$) $\mu$s. Line broadenings of 0.20 ($^{1}H$), 2.0 ($^{13}C$), 0.0 ($^{15}N$), and 1.0 ($^{19}F$) Hz were used in the exponential multiplications of the free induction decays prior to their Fourier transformations. Gaussian multiplication of the free induction decay was applied to observe the natural abundance $^{187}Os$ satellites in the $^{19}F$ NMR spectrum of *fac*-$OsO_3F_2(NCCH_3)$ recorded in $SO_2ClF$ solvent at −80 °C.

The $^{1}H$, $^{13}C$, $^{15}N$, and $^{19}F$ spectra were referenced externally at 30 °C to samples of neat liquid $(CH_3)_4Si$ ($^{1}H$ and $^{13}C$), $CH_3NO_2$, and $CFCl_3$, respectively. The chemical shift convention used is that a positive (negative) sign indicates a chemical shift to high (low) frequency of the reference compound.

**Raman Spectroscopy.** The low-temperature Raman spectra of *fac*-$OsO_3F_2(NCCH_3)$ (−150 °C) and *fac*-$OsO_3F_2(NCCH_3)\cdot nCH_3CN$ ($n \geq 2$) were recorded in ¼-in. o.d. sample tubes on a Bruker RFS 100 FT Raman spectrometer using 1064-nm excitation and a resolution of 1 $cm^{-1}$ as previously described.[3] The spectra were recorded using a laser power of 300 mW and a total of 1200 and 300 scans, respectively.

**X-ray Structure Determination of *fac*-$OsO_3F_2(NCCH_3)\cdot 2CH_3CN$. (a) Crystal Growth.** Crystals of *fac*-$OsO_3F_2(NCCH_3)\cdot 2CH_3CN$ were obtained from a sample composed of 0.021 g (0.076 mmol) of $(OsO_3F_2)_\infty$ and excess (ca. 0.2 mL) $CH_3CN$ in a ¼-in. o.d. FEP beaded reactor with three wells for crystal growth.[40] The reactor was warmed to −40 °C, whereupon $(OsO_3F_2)_\infty$ dissolved, forming a yellow-brown solution. The reactor was placed in a horizontal position, distributing the $CH_3CN$ solution among the three wells that had been blown into the FEP vessel. The solution was maintained between −41 and −45 °C over 6 h, resulting in the growth of light orange blocks while the supernatant solution retained its yellow-brown color. The orange blocks were isolated by removal of the supernatant through a Teflon cannula using an overpressure of argon,[50] followed by evacuation and drying of the crystalline product under dynamic vacuum at −45 °C for 10 min. A crystal having the dimensions 0.23 × 0.12 × 0.09 $mm^3$ was selected at −105 ±3 °C for low-temperature X-ray structure determination and was mounted in a cold stream (−173 °C) on a goniometer head as previously described.[3]

**(b) Collection and Reduction of X-ray Data.** The crystal was centered on a Bruker SMART APEX II diffractometer, equipped with an APEX II 4K CCD area detector and a triple-axis goniometer, controlled by the APEX2 Graphical User Interface (GUI) software,[51] and a sealed source emitting graphite-monochromated Mo−Kα radiation ($\lambda$ = 0.71073 Å). Diffraction data collection (at −173 °C) consisted of a full $\phi$-rotation at a fixed $\chi$ = 54.74° with 0.36° (1010) frames, followed by a series of short (250 frames) $\omega$ scans at various $\phi$ settings to fill the gaps. The crystal-to-detector distance was 4.953 cm, and the data collection was carried out in a 512 × 512 pixel mode using 2 × 2 pixel binning. Processing of the raw data was completed by using the APEX2 GUI software,[51] which applied Lorentz and polarization corrections to the three-dimensionally integrated diffraction spots. The program SADABS[52] was used for the scaling of diffraction data, the application of a decay correction, and an empirical absorption correction on the basis of the intensity ratios of redundant reflections.

**(c) Solution and Refinement of the Structure.** The XPREP[53] program was used to confirm the unit cell dimensions and the crystal lattice. The solution was obtained by direct methods which located the positions of the atoms defining $OsO_3F_2$ and the carbon and nitrogen atoms of the $CH_3CN$ molecules. The positions of the hydrogen atoms of the adducted $CH_3CN$ molecule were calculated, and the hydrogen atoms of the free $CH_3CN$ molecule were found in the difference map. The final refinement was obtained by introducing anisotropic thermal parameters and the recommended weightings for all atoms. The maximum electron densities in the final difference Fourier map were located near the heavy atoms. All calculations were performed using the SHELXTL-plus package[53] for the structure determination, solution refinement, and molecular graphics. The initial choice of space group, *Pnma* (62), suggested by XPREP, was confirmed by PLATON from the winGX software package.[54]

**Computational Methods.** The optimized geometries and frequencies of *fac*-$OsO_3F_2(NCCH_3)$, *mer*-$OsO_3F_2(NCCH_3)$, and $CH_3CN$ were calculated at the SVWN and B3LYP[55] levels. The Stuttgart semirelativistic large core and effective core pseudopotential basis sets (SDDall) augmented for F and O with two d-type polarization functions by Huzinaga[56] were used for the SVWN level. At the B3LYP level, the Stuttgart effective core potential with the corresponding basis set augmented by one f-type polarization function ($\alpha_f$ Os 0.886)[57] was used for osmium and the aug-cc-pVTZ basis sets were used for hydrogen, carbon, nitrogen, oxygen, and fluorine. Pseudopotentials were used with the Stuttgart basis set for osmium. For the attempted optimization of *cis*, *trans*-$OsO_3F_2$, aug-cc-pVTZ basis sets for F and O were used, and the aug-cc-pVTZ-PP basis set for osmium was used. Their combined use is indicated by aug-cc-pVTZ(-PP). Quantum-chemical calculations were carried out using the program Gaussian 03.[58] The levels and basis sets were benchmarked by calculating *cis*-$OsO_2F_4$[23] and $CH_3CN$[11] as previously described. The geometries were fully optimized using analytical gradient methods. After optimization at one level of theory, the geometries were calculated at the other level of theory to ensure an equivalent energy-minimized geometry

(50) Brock, D. S.; Bilir, V.; Mercier, H. P.; Schrobilgen, G. J. *J. Am. Chem. Soc.* **2007**, *129*, 3598–3611.

(51) *APEX2*, Release 2.0-2; Bruker AXS Inc.: Madison, WI, 2005.

(52) Sheldrick, G. M. *SADABS, Siemens Area Detector Absorption Corrections*, version 2.10; Siemens Analytical X-ray Instruments Inc.: Madison, WI, 2004.

(53) Sheldrick, G. M. *SHELXTL-Plus*, release 6.14; Siemens Analytical X-ray Instruments, Inc.: Madison, WI, 2000−2003.

(54) Farrugia, L. J. *J. Appl. Crystallogr.* **1999**, *32*, 837–838.

(55) Frisch, M. J. et al. *Gaussian 03*, Revision B.04; Gaussian, Inc.: Pittsburgh, PA, 2003.

(56) Huzinaga, S.; Andzelm, J.; Kolobukowski, M.; Radzio-Andzelm, E.; Sakai, Y.; Tatewaki, H. *Gaussian Basis Sets for Molecular Calculations*; Physical Science Data 16; Elsevier: Amsterdam, 1984.

(57) Ehlers, A. W.; Böhme, M.; Dapprich, S.; Gobbi, A.; Höllwarth, A.; Jonas, V.; Köhler, K. F.; Stegmann, R.; Veldkamp, A.; Frenking, G. *Chem. Phys. Lett.* **1993**, *208*, 111–114.

(58) Frisch, M. J. et al. *Gaussian 98*, Revision A.11; Gaussian, Inc.: Pittsburgh, PA, 2003.

had been achieved. The vibrational frequencies were calculated at the SVWN and B3LYP levels using the appropriate minimized structure, and the vibrational mode descriptions were assigned with the aid of Gaussview.[59]

**Acknowledgment.** We thank the Natural Sciences and Engineering Research Council of Canada for the award of postgraduate scholarships (M.J.H.) and for support in the form of a Discovery Grant (G.J.S.). We also thank the Ontario Ministry of Education and the Richard Fuller and James A. Morrison Memorial Funds for the award of graduate scholarships (M.G.). The calculations were conducted with the aid of the facilities of the Shared Hierarchical Academic Research Computing Network (SHARCNET: www.Sharcnet.ca).

**Supporting Information Available:** Raman spectra acquired during the removal of $CH_3CN$ from a $CH_3CN$ solution of *fac*-$OsO_3F_2(NCCH_3)$, and the Raman spectra of uncoordinated $CH_3CN$ and of *fac*-$OsO_3F_2(NCCH_3)$ isolated from $SO_2ClF$ (Table S1); unit cell of *fac*-$OsO_3F_2(NCCH_3)\cdot 2CH_3CN$ viewed along the *a*-axis (Figure S1); Raman spectrum of $OsO_3F_2(NCCH_3)\cdot nCH_3CN$ (Figure S2); factor-group analysis for *fac*-$OsO_3F_2(NCCH_3)\cdot 2CH_3CN$ (Table S2); calculated gas-phase geometry (SVWN) for $CH_3CN$ (Figure S3); natural bond orbital (NBO) valencies, bond orders, and natural population analysis (NPA) charges for *fac*-$OsO_3F_2(NCCH_3)$, *mer*-$OsO_3F_2(NCCH_3)$, and $CH_3CN$ (Table S3); calculated vibrational frequencies, intensities, and assignments for *fac*- and *mer*-$OsO_3F_2(NCCH_3)$ (Table S4); calculated gas-phase $\Delta H$ and $\Delta G$ values for the conversion of *fac*-$OsO_3F_2(NCCH_3)$ to *mer*-$OsO_3F_2(NCCH_3)$ (Table S5); complete references 55 and 58; and the X-ray crystallographic file in CIF format for the structure determination of $OsO_3F_2(NCCH_3)\cdot 2CH_3CN$. This material is available free of charge via the Internet at http://pubs.acs.org.

(59) *GaussView*, release 3.0; Gaussian Inc.: Pittsburgh, PA, 2003.